1 **Release of Notch activity coordinated by IL-1β signalling confers differentiation plasticity**

2 **of airway progenitors via Fosl2 during alveolar regeneration**

3

4 Jinwook Choi[1,10], Yu Jin Jang[2,10], Catherine Dabrowska[1,3], Elhadi Iich[1], Kelly V. Evans[1,3],

5 Helen Hall[4], Sam M. Janes[4], Benjamin D. Simons[1,5,6], Bon-Kyoung Koo[7], Jonghwan Kim[2,8,9,*],

6 and Joo-Hyeon Lee[1, 3,*,#]

7

8 [1]Wellcome – MRC Cambridge Stem Cell Institute, Jeffrey Cheah Biomedical Centre,

9 University of Cambridge, Cambridge, CB2 0AW, UK

10 [2]Department of Molecular Biosciences, The University of Texas at Austin, Austin, TX, 78712,

11 USA.

12 [3]Department of Physiology, Development and Neuroscience, University of Cambridge,

13 Cambridge, CB2 3EL, UK

14 [4]Lungs for Living Centre, UCL Respiratory, Division of Medicine, University College London,

15 WC1E 6JF, UK

16 [5]Wellcome – Cancer Research UK Gurdon Institute, University of Cambridge, Cambridge,

17 CB2 1QN, UK

18 [6]Department of Applied Mathematics and Theoretical Physics, Centre for Mathematical

19 Science, University of Cambridge, Cambridge, CB3 0WA, UK

20 [7]Institute of Molecular Biotechnology of the Austrian Academy of Science (IMBA), Vienna

21 Biocenter (VBC), Dr. Bohr-Gasse 3, 1030, Vienna, Austria

22 [8]Institute for Cellular and Molecular Biology, The University of Texas at Austin, Austin, TX,

23 78712, USA

24 [9]Center for Systems and Synthetic Biology, The University of Texas at Austin, Austin, TX,

25 78712, USA

26 [10]First author

27 *Correspondence

28 #Lead contact

29

30

31 Contact information

32 Email: jhl62@cam.ac.uk

33

34   **Abstract**

35   While the acquisition of cellular plasticity in adult stem cells is essential for rapid regeneration

36   after tissue injury, little is known about the underlying molecular mechanisms governing this

37   process. Our data reveal the coordination of airway progenitor differentiation plasticity by

38   inflammatory signals during alveolar regeneration. Upon damage, IL-1β signalling-dependent

39   modulation of Jag1/2 expression in ciliated cells results in the inhibition of Notch signalling in

40   secretory cells, which drives reprogramming and acquisition of differentiation plasticity. We

41   identify a core role for the transcription factor Fosl2/Fra2 in secretory cell fate conversion to

42   alveolar type 2 (AT2) cells retaining the distinct genetic and epigenetic signatures of secretory

43   lineages. We furthermore reveal that KDR/FLK-1$^+$ human secretory cells display a conserved

44   capacity to generate AT2 cells via Notch inhibition. Our results demonstrate the functional role

45   of a IL-1β-Notch-Fosl2 axis for the fate decision of secretory cells during injury repair,

46   proposing a new potential therapeutic target for human lung alveolar regeneration.

47

48

49

2

50 **Main**

51 Tissue homeostasis is maintained by stem and progenitor cells capable of self-renewal and

52 lineage-restricted differentiation, governed by specialised microenvironments. Both stem and

53 progenitor cells acquire a remarkable potential for multi-lineage differentiation after tissue

54 insults to allow for rapid regeneration of damaged tissue[1,2]. These capacities depend on the

55 nature and/or extent of injury, the repair ability of resident stem/progenitor cells, and their local

56 microenvironments. Dysregulation of cellular plasticity, however, leads to lineage infidelity,

57 and is implicated in various diseases[2]. Thus, to understand the process of tissue repair and

58 regeneration in homeostasis and pathology, it is important to elucidate how stem and progenitor

59 cells sense damage signals and control transient plasticity for fate conversion.

60

61 Lung tissue is maintained by several stem and progenitor cell types that reside in anatomically

62 distinct regions alongside the pulmonary axis[3,4]. In the distal lungs two main stem cell types,

63 secretory cells and alveolar type 2 (AT2) cells, separately maintain the airway and alveolar

64 epithelium compartments, respectively. In alveolar homeostasis and injury conditions, AT2

65 cells have been identified as the resident alveolar stem cells capable of self-renewal and

66 differentiation into alveolar type 1 (AT1) cells[5-7]. However, when alveolar integrity is severely

67 disrupted following lung injury, such as bleomycin or influenza infection, stem/progenitor cells

68 localised in the distal airway (including secretory cells) can contribute to alveolar regeneration

69 by differentiating into AT2 cells[5,6,8-12]. In particular, several lines of evidence reveal the

70 capacity of lineage-traced *Scgb1a1+* airway secretory cells, which exhibit restricted capacity

71 to generate airway cells in homeostasis, to produce new AT2 cells following severe lung injury

72 in order to achieve effective repair of the alveolar epithelium[5,6]. However, little is known about

73 the cellular events and molecular cues which dictate how secretory cells lose their identity in

74 response to alveolar damage and subsequently acquire AT2 cell fate. Significantly, the chronic

75 loss of alveolar integrity is strongly associated with various human lung diseases. Thus, it is

76 imperative to understand whether there is a functionally conserved secretory cell population

77 that readily mediates human alveolar regeneration, and whether regulatory mechanisms are

78 conserved between human and mouse lungs.

79

80 Here, we establish chemically defined feeder-free *in vitro* organoid cultures wherein secretory

81 cells and AT2 cells are capable of expansion with a restricted differentiation capacity. This

82 platform enables us to perform robust interrogation of the molecular and cellular behaviour of

83 secretory and AT2 cells *in vitro*. By comparing the gene expression patterns in these organoids,

3

84   we identify the Notch signalling pathway as a pivotal regulator for the differentiation plasticity

85   of secretory cells into AT2 cells. We demonstrate the role of IL-1β-mediated inflammation in

86   ciliated cells in regulating this differentiation plasticity *in vivo*. The AP-1 transcription factor

87   Fosl2/Fra2 is defined as an essential transcription factor for AT2 cell conversion from secretory

88   cells in response to Notch signalling. Further, the distinct genetic and epigenetic signatures of

89   secretory-derived AT2 cells confer their functional difference compared to resident AT2 cells.

90   Lastly, we demonstrate that the role of Notch signalling in the transition of secretory cells to

91   AT2 cells is conserved in human airway organoids derived from KDR/FLK-1^{+} secretory cells.

92   Our study illustrates the precise molecular and cellular coordination required for secretory cell-

93   mediated alveolar regeneration, providing new insights into both the potential regenerative

94   roles of these cells and regulatory networks in repairing alveolar destruction in lung disease.

95

96   **Results**

97   **Establishment of *in vitro* feeder-free self-renewing culture conditions for distal stem cells**

98   To better understand and more easily manipulate lung epithelial stem cells, we established a

99   simple feeder-free organoid culture condition with defined factors which support the molecular

100   and functional identity of stem cells over long-term culture. Airway secretory cells expressing

101   *Scgb1a1* (*Secretoglobin 1a1*, also known as *CC10* or *CCSP*) were isolated from the distal lung

102   tissues of secretory cell reporter mice (*Scgb1a1-CreER[TM/+];R26R[tdTomato/+]*) after tamoxifen

103   treatment[13] (Fig. 1a). Lineage-labelled secretory cells were embedded in Matrigel

104   supplemented with WNT3A, RSPO1 (R-spondin 1), EGF, FGF7, FGF10, and NOG (Noggin),

105   factors that are known to support the growth of human embryonic lung tip cells and progenitors

106   derived from foregut lineages[14-18] (Fig. 1b). Under this condition, we were able to grow

107   secretory cells that formed cyst-like organoids (Fig. 1b). The organoids were capable of long-

108   term expansion (>2 years) by dissociation into single cells with stable forming efficiency (Fig.

109   1c,d). We also successfully generated organoids after limiting dilution with drops containing

110   single cells (Fig. 1e), which serves as evidence of the clonogenicity and stem cell property of

111   secretory cells maintained in this condition. FGF10 was dispensable for organoid growth with

112   no significant difference in the efficiency of organoid formation and maintenance over serial

113   passages (Fig. 1b-d). Without FGF7, however, secretory cells failed to form organoids (Fig.

114   1b,d). Furthermore, the absence of factors supporting WNT activity resulted in deterioration of

115   organoid expansion over passages (Fig. 1b,d), indicating that both FGF7 and WNT signalling

116   are essential for the self-renewal of distal secretory cells. The initial organoid cultures retained

117   heterogeneous phenotypes of organoids, including airway retaining CC10^{+} secretory and

118   Acetylated-Tubulin (Act-Tub)$^+$ ciliated cells, alveolar retaining SPC$^+$ AT2 and HOPX$^+$ AT1

119   cells, and mixed organoids retaining both airway and alveolar lineage cells, similar to previous

120   findings from the co-culture system[19] (Fig. 1f,i). After five passages, organoids expanded to

121   form mainly mixed organoids with budding-like morphology over multiple passages (Fig. 1g-

122   i).

123

124   We next asked whether our culture condition could allow AT2 cells to form organoids.

125   Lineage-labelled AT2 cells were isolated from *Sftpc-CreER$^{T2/+}$;R26R$^{tdTomato/+}$* reporter mice

126   after tamoxifen treatment[5] (Extended Data Fig. 1a). Like secretory cell-derived organoids

127   (referred to here as SCOs), they were capable of forming cyst-like organoids (Extended Data

128   Fig. 1b). Consistent with previous studies[20-23], FGF7 and WNT activity were essential for

129   forming and maintaining AT2 cell-derived organoids (referred to hereafter as ACOs), which

130   contained both SPC$^+$ AT2 and Pdpn$^+$ AT1 cells (Extended Data Fig. 1b-f). We also confirmed

131   the clonogenic ability of AT2 cells by organoid culture with single cells (Extended Data Fig.

132   1e). However, unlike SCOs, which tolerate the presence of FGF10 in long-term culture, ACOs

133   were better maintained in the absence of FGF10 (Extended Data Fig. 1d). After several

134   passages, these organoids expanded to form alveolar-like structures that were mainly composed

135   of AT2 cells with little AT1 cell differentiation (Extended Data Fig. 1g,h). Taken together, we

136   developed a feeder-free organoid culture system with chemically defined medium, wherein

137   distal airway secretory cells and AT2 cells were maintained with stem cell activity in long-

138   term cultures. Activation of both FGF7 and WNT signalling pathways was sufficient to support

139   them.

140

141   **Inhibition of Notch signalling confers plasticity of secretory cells to differentiate into AT2**

142   **cells upon injury**

143   To investigate the characteristics of SCOs and ACOs, we first performed bulk RNA-seq

144   analysis. Consistent with immunofluorescent (IF) staining data, SCOs exhibited a distinct gene

145   expression pattern enriched in secretory cell markers such as *Scgb1a1*, *Cyp2f2*, and *Gabrp*,

146   while AT2 cell markers including *Sftpc* and *Etv5* were highly expressed in ACOs (Fig. 2a). In

147   addition, gene set enrichment analysis (GSEA) revealed that secretory cell marker genes were

148   enriched in the genes highly active in SCOs, whereas AT2 cell markers were enriched in ACOs

149   (Fig. 2b). Notably, GSEA indicated that Notch signalling was distinctly enriched in SCOs (Fig.

150   2b). We also confirmed that the expression of genes regulated by Notch signalling, such as

151   *Hes1*, *Hes6* and *Nrarp*, was upregulated in SCOs compared to ACOs (Fig. 2a). Additional IF

5

152 staining also confirmed the expression of intracellular domain of Notch1 (N1ICD) in SCOs
153 (Extended Data Fig. 2a). This observation prompted us to examine whether Notch signalling
154 is involved in the identity and fate behaviour of secretory cells. We dissociated established
155 SCOs into single cells and replated them to form organoids in the presence of DMSO (control)
156 or DAPT, a γ-secretase inhibitor, to inhibit Notch signalling. Remarkably, SPC$^+$ AT2 cells
157 were dramatically increased at the expense of CC10$^+$ secretory cells in DAPT-treated organoids
158 compared to control, whereas other lineages were barely affected (Fig. 2c). To further
159 characterise these organoids, we performed RNA-seq analysis of SCOs with and without
160 DAPT treatment. Unlike control organoids, DAPT-treated organoids displayed strongly
161 upregulated AT2 cell marker gene expression and a substantial reduction of secretory cell
162 markers (Fig. 2d). GSEA also showed similar expression patterns (Fig. 2e). To directly confirm
163 the functional effect of Notch activity in secretory cells, we knocked-down *Rbpj*, the major
164 transcriptional effector of Notch signalling, in SCOs. Knockdown (KD) of *Rbpj* promoted the
165 differentiation of secretory cells into AT2 cells without DAPT treatment (Extended Data Fig.
166 2b,c), suggesting that inhibition of Notch signalling triggers the conversion of secretory cells
167 into AT2 lineage.

168

169 To address this finding *in vivo*, we used mice carrying a conditional dominant-negative mutant
170 of mastermind-like 1 (dnMAML$^{flox/flox}$)[24], which inhibits NICD-induced Notch signalling,
171 crossed with *Scgb1a1-CreER$^{TM/+}$;R26R$^{tdTomato/+}$*. Control (*Scgb1a1-CreER$^{TM/+}$;R26R$^{tdTomato/+}$*)
172 or dnMAML$^{flox/+}$ (*dnMAML$^{flox/+}$;Scgb1a1-CreER$^{TM/+}$;R26R$^{tdTomato/+}$*) mice were exposed to
173 PBS or bleomycin after tamoxifen treatment to induce alveolar injury (Fig. 2f). Inhibition of
174 Notch activity by *dnMAML* expression was confirmed by assessing the expression of Hes1, a
175 potent target gene of Notch signalling (Extended Data Fig. 2d,e). Consistent with previous
176 studies[25-27], the proportion of lineage-labelled ciliated cells was increased by Notch inhibition
177 in dnMAML$^{flox/+}$ compared to control mouse lungs (Extended Data Fig. 2f,g). As reported[13],
178 6.23±1.09% of lineage-labelled AT2 cells were observed in the alveolar region of uninjured
179 control lung (Fig. 2g,i). The percentage of Tomato$^+$AT2 cells (6.97±13.12%) in uninjured lung
180 of dnMAML$^{flox/+}$ mice was similar to that seen in control mice (Fig. 2g,i). However, bleomycin
181 injury significantly increased the population of lineage-labelled AT2 cells to 25.24±8.08% in
182 control mice (Fig. 2h,i). Importantly, we observed a substantial increase in lineage-labelled
183 AT2 cells (56.39±12.91%) post injury in dnMAML$^{flox/+}$ mice (Fig. 2h,i), suggesting that
184 persistent inhibition of Notch signalling in secretory cells enhances their differentiation
185 towards AT2 cell fate during injury repair. Further analysis of *in vitro* organoids also

6

186   demonstrated that *dnMAML*-expressing secretory cells enhanced the frequency of formation of

187   alveolar organoids retaining AT2 cells and reduced occurrence of airway organoids retaining

188   secretory cells (Extended Data Fig. 3). Moreover, pharmacological inhibition of Notch activity

189   by DAPT treatment *in vivo* also showed a significant increase of AT2 cells derived from

190   secretory cells (Extended Data Fig. 4).

191

192   Given that *Scgb1a1*$^+$ lineage-labelled cells contained heterogeneous populations, including

193   CC10$^+$SPC$^+$ dual-positive cells, we further evaluated the differentiation capacity of lineage-

194   labelled secretory cells into AT2 lineages via Notch inhibition after excluding lineage-labelled

195   SPC$^+$AT2 cells. We isolated lineage-labelled secretory cells (EpCAM$^+$Tomato$^+$MHCII$^-$) from

196   control and dnMAML$^{flox/+}$ mouse lungs, followed by transplantation into the lungs after

197   bleomycin injury (Extended Data Fig. 5a,b). Secretory cells isolated from dnMAML$^{flox/+}$ lungs

198   showed enhanced ability to generate AT2 cells compared to control secretory cells (Extended

199   Data Fig. 5c-h). We also confirmed that *dnMAML*-expressing secretory cells revealed the

200   greater frequency of alveolar organoid formation compared to control secretory cells (Extended

201   Data Fig. 5i). Taken together, our data strongly suggest that persistent inhibition of Notch

202   signalling enhances the differentiation of secretory cells into AT2 cells post injury.

203

204   **Sustained activation of Notch signalling impairs the differentiation of secretory cells into**

205   **AT2 cell fate during alveolar injury repair**

206   We then asked whether the constitutive activation of Notch signalling affects the cell fate of

207   secretory cells upon injury. To this end, we used *Red2-Notch^{N1ICD}* mice, where constitutive

208   *N1ICD* is specifically co-expressed in *tdimer2 red fluorescent protein* (RFP)$^+$ cells in the

209   original confetti mouse line (Yum *et al.*, in press) (Fig. 3a). The other three lineage outcomes,

210   namely YFP, GFP and CFP, all represent wild-type events. In *in vitro* organoid cultures of

211   YFP$^+$ (wild-type, control) and RFP$^+$ (constitutive *N1ICD*) cells, RFP$^+$ cells showed a

212   significant increase in organoid formation efficiency compared to that of YFP$^+$ cells (Fig. 3b,c).

213   Consistent with previous results (Extended Data Fig. 3), YFP$^+$ control cells gave rise to three

214   distinct types of organoids in co-cultures (Fig. 3d,e). However, only airway organoids arose

215   from RFP$^+$ cells (Fig. 3d,e). To further investigate the cellular behaviour of secretory cells with

216   constitutive Notch activity *in vivo*, *Scgb1a1-CreER$^{TM/+}$;Red2-Notch$^{N1ICD/+}$* mice were

217   administered PBS or bleomycin injury (Fig. 3a). In uninjured lungs, YFP$^+$ and RFP$^+$ cells were

218   localised in airways with the expression of the secretory cell marker CC10, and no lineage-

219   labelled cells were observed in the alveolar region (Fig. 3f,h and Extended Data Fig. 5j). After

220   bleomycin injury, we observed an increased frequency of YFP$^+$ lineage-labelled AT2 cells

221   expressing SPC in the alveolar regions (Fig. 3g-i). However, an increase of RFP$^+$ lineage-

222   labelled AT2 cells was significantly compromised after injury (Fig. 3g-i). Although RFP$^+$ cells

223   also expanded post injury, they still maintained identity of secretory cells retaining CC10

224   expression (Fig. 3g-i).

225

226   We next sought to define the molecular identity and characteristics of YFP$^+$ or RFP$^+$ cells

227   during alveolar regeneration. To this end, we carried out single-cell RNA-sequencing (scRNA-

228   seq) analysis by isolating lineage-labelled (YFP$^+$ or RFP$^+$) and non-lineage-labelled (YFP$^-$

229   RFP$^-$) populations at day 28 post bleomycin injury (Extended Data Fig. 6a). Based on the

230   expression of canonical markers for specific cell types, we revealed 14 distinct populations

231   (Extended Data Fig. 6b,c). To gain insight into the impact of Notch activity on lineage

232   differentiation of secretory cells into AT2 cells, we further analysed the secretory and AT2 cell

233   populations (Fig. 3j). This analysis uncovered four distinctive clusters, including three different

234   types of secretory cells and an AT2 cell cluster (Fig. 3j,k). In addition to the known secretory

235   cell populations, including *Scgb3a2^{high}* canonical secretory cells (cluster 1) and *H2-K1^{high}* cells

236   (cluster 2)[8] sharing common secretory markers (e.g. *Cldn10*), our analysis identified an

237   uncharacterized population which we termed *Fstl1$^+$* secretory cells (cluster 3; Fig. 3j,k). While

238   cells in this cluster still retained the identity of secretory cells based on *Scgb1a1* expression,

239   they showed lower expression levels of some secretory cell markers such as *Scgb3a2* and

240   *Cldn10* (Fig. 3k). Moreover, this cluster was marked by specific expression of discrete markers

241   such as *Id3* and *Porcn* (Fig. 3k). Interestingly, this population had elevated expression of

242   *Cdkn1c*/p57, involved in cell cycle inhibition, which could indicate the quiescent

243   characteristics of this cluster *in vivo* (Fig. 3k and Extended Data Fig. 6d,e). Distribution of each

244   cluster across collected samples allowed us to assess how control (YFP$^+$) or *N1ICD*-expressing

245   (RFP$^+$) cells respond to injury. Consistent with lineage-tracing analysis, control YFP$^+$ cells

246   contributed to alveolar regeneration by giving rise to AT2 cells post injury (Fig. 3l). However,

247   RFP$^+$ cells were arrested at the stage of the *Fstl1$^+$* population, causing impaired differentiation

248   into AT2 cells (Fig. 3l). Pseudotime analysis revealed that the transition from secretory cells

249   to AT2 cells is mediated via this cluster 3, suggesting that this population may function as a

250   transitional intermediate in the lineage transition between secretory cells and AT2 cells, and

251   inactivation of Notch activity is required for the transition of this intermediate state into AT2

252   cell fate (Extended Data Fig. 6f). Overall, our results indicate that sustained activation of Notch

253 signalling causes defects in alveolar regeneration by blocking the fate conversion from
254 secretory cells to AT2 cells.

255

256 **IL-1β signalling in ciliated cells is required for Notch-dependent fate conversion of**
257 **secretory cells to AT2 cells after injury**

258 We next asked how Notch activity in secretory cells is regulated during regeneration. Given
259 that Notch signalling involves short-range cellular communication through direct contact by
260 receptor-ligand interaction, we examined which cells highly express the Notch ligands Jagged
261 1 (Jag1) and Jagged 2 (Jag2). Our scRNA-seq analysis from *Scgb1a1-CreER^(TM/+)*;*Red2-*
262 *Notch^(N1ICD/+)* mice revealed that *Jag1* and *Jag2* are highly expressed in ciliated cells, which
263 reside adjacent to secretory cells in the airway, consistent with previous studies[27-29] (Extended
264 Data Fig. 7a,b). Immunohistochemistry (IHC) staining also confirmed the high expression of
265 Jag1 in ciliated cells (Extended Data Fig. 7c). Notably, we found that Jag1 expression was
266 downregulated after bleomycin treatment, suggesting dynamic modulation of Notch signalling
267 by ciliated cells during injury repair (Extended Data Fig. 7c). Previously we showed dynamic
268 expression of IL-1β during regeneration after bleomycin injury[30]. Notably, *Il1r1*, a functional
269 receptor for IL-1β, is specifically expressed in ciliated cells, in addition to subsets of AT2 cells
270 (Extended Data Fig. 7d,e)[30]. Thus, we asked whether IL-1β signalling modulates the expression
271 of Notch ligands in ciliated cells. The expression of Notch ligands, *Jag1* and *Jag2*, was
272 significantly reduced in *Il1r1^+* ciliated cells (EpCAM^+*Il1r1*^+CD24^high) after bleomycin injury
273 compared to PBS control (Fig. 4a,b). Furthermore, we treated PBS or IL-1β in isolated *Il1r1^+*
274 ciliated cells for 24 hours. The expression of *Jag1* and *Jag2* was significantly downregulated
275 in IL-1β-treated ciliated cells compared to control cells, suggesting that IL-1β signalling
276 directly modulates the expression of Notch ligands in ciliated cells after injury (Fig. 4c).

277

278 We next asked whether depletion of IL-1β signalling on ciliated cells impacts the fate
279 behaviour of secretory cells after injury *in vivo*. To delete *Il1r1* in ciliated cells and lineage-
280 trace secretory cells simultaneously, we established *Il1r1^(flox/flox)*;*Foxj1-CreER^(T2)* mice crossed
281 with *Scgb1a1-CreER^(TM)*;*R26^(RtdTomato)* mice (Fig. 4d). Of note, in the distal airway, *Il1r1* only
282 marks ciliated cells, not secretory cells[30]. Moreover, ciliated cells are known to lack hallmark
283 features of progenitor cells including self-renewal activity and generation of other lineages,
284 including secretory and AT2 cells, which was also supported by our organoid assay (Extended
285 Data Fig. 7f)[30-32]. Given these pieces of evidence, we examined the expression of Notch ligands
286 (*Jag1*, *Jag2*, *Dll1*, *Dll4*) in ciliated cells of *Il1r1^(flox/flox)*;*Scgb1a1-CreER^(T2/+)*;*R26^(RtdTomato/+)* mice

9

287   after PBS or bleomycin treatment. Consistently, qPCR analysis revealed significant

288   downregulation of *Jag1/2* expression in ciliated cells after injury, indicating a transient

289   reduction in Notch activity as an initial step in secretory cell-mediated regeneration after injury

290   (Fig. 4e). However, ciliated cells of *Foxj1-CreER^{T2}*;*Il1r1^{flox/flox}*;*Scgb1a1-*

291   *CreER^{T2/+}*;*R26^{RtdTomato/+}* mice failed to downregulate the expression of these ligands after

292   bleomycin treatment, suggesting that IL-1β signalling via *Il1r1* mediates the reduction of

293   *Jag1/2* expression in ciliated cells after injury (Fig. 4e). Significantly, after injury, Notch

294   activity was reduced in secretory cells, which was impaired by *Il1r1* deletion in ciliated cells

295   (Fig. 4f-h). We then checked the lineage behaviour of lineage-labelled cells in these mice at

296   day 28 after injury. There was no discernible alteration in lineage-labelled cells by *Il1r1*

297   deletion in ciliated cells in PBS control lungs (Extended Data Fig.7g-i). However, we found a

298   significant reduction in the frequency of lineage-labelled AT2 cells in the lungs of *Foxj1-*

299   *CreER^{T2}*;*Il1r1^{flox/flox}*;*Scgb1a1-CreER^{T2/+}*;*R26^{RtdTomato/+}* mice compared to the lungs of

300   *Il1r1^{flox/flox}*;*Scgb1a1-CreER^{T2/+}*;*R26^{RtdTomato/+}* mice after bleomycin injury (Fig. 4i,j). Taken

301   together, these data indicate that IL-1β signals build niche environments governing the

302   expression of Notch ligands, Jag1 and Jag2, in ciliated cells, which is essential for the fate

303   transition of secretory cells toward AT2 cells during alveolar regeneration.

304

305   **Fosl2-mediated AP-1 transcription factor is required for the fate conversion of secretory**

306   **cells into AT2 cells**

307   To investigate the epigenetic regulation that mediates the differentiation of secretory cells into

308   AT2 cells, we performed ATAC-seq (Assay for Transposase-Accessible Chromatin with high-

309   throughput sequencing) with secretory and secretory-derived AT2 cells (referred to as sAT2

310   from here). We generated *Sftpc-dsRed^{IRES-DTR}* AT2 reporter mice to monitor SPC-expressing

311   AT2 cells and crossed them with the *Scgb1a1-CreER^{TM}*;*R26R^{fGFP}* mice to trace cells derived

312   from secretory cells after bleomycin injury (Fig. 5a). As expected, lineage-labelled sAT2 cells

313   (GFP^{+}dsRed^{+}) were increased compared to control at day 28 post injury (Extended Data Fig.

314   7j). For ATAC-seq analysis, we isolated lineage-labelled secretory (GFP^{+}dsRed^{−}) and sAT2

315   (GFP^{+}dsRed^{+}) cells (Fig. 5a,b). We identified a total of 54,845 and 52,763 peaks in secretory

316   and sAT2 cells, respectively (Fig. 5c). Spearman correlation coefficients showed the high

317   correlation between biological replicates (Extended Data Fig. 8a). The distribution of peaks

318   from secretory and sAT2 cells were similarly represented, and more than half of them fell into

319   enhancers (intron, exon, and distal intergenic elements) (Extended Data Fig. 8b). While

320   approximately 45,548 peaks were common, 9297 and 7316 peaks were mapped as cell-type

321   specific to secretory and sAT2 cells, respectively (Fig. 5c and Extended Data Fig. 8c). Analysis

322   of Gene Ontology (GO) terms with the genes associated with cell-type specific ATAC-seq

323   peaks revealed the distinct characteristics of secretory or AT2 cells (Extended Data Fig. 8d).

324   Indeed, known-secretory cell markers, such as *Gabrp* and *Cyp2f2*, were associated with

325   secretory cell specific-differential peaks, whereas AT2 cell markers, such as *Sftpc* and *Lyz2*,

326   were associated with sAT2 cell-specific peaks (Extended Data Fig. 8e).

327

328   We sought to identify transcription factors (TFs) that regulate these differential regions of

329   peaks by analysing TF binding motifs. Motif analysis of DNA binding-site showed that sAT2-

330   enriched chromatin contains motifs for key transcriptional factors associated with lung

331   development, including Nkx2-1 and Fosl2[33,34] (Fig. 5d). We compared the expression of TFs

332   obtained from motif analysis with RNA-seq data of control and DAPT-treated SCOs (Fig. 2d).

333   The heatmap showed that TFs in sAT2-enriched open chromatin were also highly expressed in

334   DAPT-treated organoids, whereas the expression levels of TFs identified in secretory cell-

335   restricted motif were higher in control organoids (Fig. 5e and Extended Data Fig. 8f). Notably,

336   we found the differential enrichment of AP-1 factor components in control and DAPT-treated

337   organoids; *c-Fos*, *Fosb*, *c-Jun*, and *Junb* in control organoids and *Jund* and *Fosl2/Fra2* in

338   DAPT-treated organoids (Fig. 5e). To interrogate the key TFs that are required for AT2 cell

339   differentiation, we established feeder-free SCOs with KD of five TFs (*Srebf2*, *Fosl2*, *Rbpjl*,

340   *Cebpa*, *Etv5*) selected from motif analysis or a list of differentially expressed genes in RNA-

341   seq analysis. We first validated the KD effect of *Cebpa* and *Etv5*, well-known factors for AT2

342   cell identity[35,36], on the fate switch of secretory to AT2 cells by exposing organoids to DAPT.

343   The upregulation of AT2 cell markers by Notch inhibition was not affected by the interference

344   of *Cebpa* or *Etv5* (Extended Data Fig. 8g,h). The KD of *Srebf2* and *Rbpjl*, which are highly

345   ranked in motif analysis, also did not impair the expression of AT2 cell markers by DAPT

346   treatment (Fig. 5f). However, remarkably, KD of *Fosl2/Fra2* significantly blocked the increase

347   of AT2 cell markers, including *Sftpc* and *Etv5*, by DAPT treatment whereas the downregulation

348   of secretory cell markers such as *Scgb1a1* was not altered (Fig. 5f). Further IF analysis also

349   confirmed impaired induction of SPC$^+$ AT2 cells in *Fosl2*-deficient secretory organoids treated

350   with DAPT (Fig. 5g). Interestingly, we found that *Fosl2* KD markedly increased Act-Tub$^+$

351   ciliated cells in DAPT-treated organoids (Fig. 5g). These data suggest that Fosl2 is a critical

352   mediator regulating the fate conversion of secretory cells to AT2 lineage upon Notch inhibition.

353

11

354 **Airway-derived AT2 cells are distinct from alveolar resident AT2 cells in genetic and**
355 **epigenetic characteristics**

356 While AT2 cells serve as stem cells to maintain the alveolar epithelium during both
357 homeostasis and regeneration, secretory cells are the major source of replenishing alveolar
358 lineages after severe alveolar damage such as bleomycin injury[5,6]. However, it remains
359 unexplored whether sAT2 cells generated after injury-repair are genetically or functionally
360 identical to resident AT2 cells (hereafter referred to as rAT2 cells) in alveoli. To address this
361 question, we further analysed the AT2 cell population in our scRNA-seq (Fig. 3j) of *Scgb1a1-*
362 *CreER^{TM/+};Red2-Notch^{N1ICD/+}* mice challenged by bleomycin injury and found that secretory
363 lineage-labelled AT2 (sAT2, YFP$^+$) and non-lineage-labelled AT2 (rAT2, RFP$^-$YFP$^-$) cells
364 were indeed segregated (Fig. 6a). Notably, sAT2 cells still retained higher expression of many
365 secretory cell markers such as *Scgb1a1*, *Cyp2f2*, and *Sox2* while the expression of AT2 markers
366 such as *Sftpc* and *Etv5* was comparable to that seen in rAT2 cells (Fig. 6b,c). We then examined
367 the epigenetic signatures of sAT2 and rAT2 cells via ATAC-seq on isolated GFP$^+$dsRed$^+$
368 (sAT2) and GFP$^-$dsRed$^+$(rAT2) cells from *Scgb1a1-CreER^{TM/+};R26R^{fGFP/+};Sftpc-dsRed^{IRES-}*
369 *^{DTR/+}* mice treated with bleomycin injury at day 28 (Extended Data Fig. 9a,b). We identified
370 52,497 shared open regions from sAT2 and rAT2 cells and 429 differential open regions of
371 sAT2 cells (Extended Data Fig. 9c). Most sAT2-specific open regions were located far away
372 from the transcription start sites (TSS), suggesting that the differential peaks co-localized with
373 contained distal enhancer regions (Extended Data Fig. 9d). Consistent with genetic signatures,
374 the regulatory regions surrounding secretory cell marker loci, including *Scgb1a1* and *Sox2*,
375 showed accessible chromatin signatures in sAT2 cells, much like in secretory cells (Fig. 6d).
376 GO term analysis with the sAT2-specific peaks also supported the enriched secretory-like
377 signature shown in Extended Data Fig. 8d (e.g. tube morphogenesis-related pathway) in sAT2
378 cells (Extended Data Fig. 9e). Importantly, we found the distinctive feature of an apoptosis-
379 related signature in sAT2 cells (Extended Data Fig. 9e). Genes involved in the negative
380 regulation of apoptotic processes (GO:0043066) were also more highly expressed in sAT2 than
381 rAT2 cells in our scRNA-seq analysis (Extended Data Fig. 9f,g). We confirmed that the *Nr4a2*
382 locus, one of the most critical anti-apoptotic regulators in the lung, is open in sAT2 cells, but
383 not in rAT2 cells[37,38] (Extended Data Fig. 9h). Furthermore, sAT2 cells showed higher
384 expression of *Slc7a11*, which is a master regulator for redox homeostasis and essential for
385 survival in response to cellular stress such as cystine deficiency, which can lead to cell death,
386 referred to as ferroptosis[39,40] (Fig. 6b).

387

12

388   Given these findings, to interrogate the functional differences between sAT2 and rAT2 cells,
389   we established organoid co-cultures of GFP+dsRed+ (sAT2) and GFP−dsRed+ (rAT2) cells
390   isolated from *Scgb1a1-CreER*$^{M2/+}$;*R26R*$^{fGFP/+}$;*Sftpc-dsRed*$^{IRES-DTR/+}$ mice at 2 months post
391   bleomycin injury. Consistent with previous research[41], rAT2 cells lost colony forming
392   efficiency (CFE) after serial passaging (Fig. 6e,f). However, sAT2 cells formed stable
393   organoids without loss of CFE over multiple passages (Fig. 6e,f). Moreover, sAT2-derived
394   organoids revealed a greater ratio of AT1 versus AT2 cells compared to that of rAT2-derived
395   organoids, suggesting enhanced differentiation capacity into AT1 lineages (Extended Data Fig.
396   9i-k). We were also able to detect sAT2 cells (GFP+dsRed+) in the lungs of *Scgb1a1-*
397   *CreER*$^{TM/+}$;*R26R*$^{fGFP/+}$;*Sftpc-dsRed* mice for least at 3 months post bleomycin injury (Extended
398   Data Fig. 9l,m). Taken together, these data indicate that AT2 cells derived from secretory cells
399   during alveolar regeneration remain functionally and epigenetically distinct compared to
400   alveolar resident AT2 cells.

401

402   **Conserved differentiation potential of human secretory cells marked by KDR/FLK-1**
403   The potential of airway cell compartments to contribute to alveolar regeneration in the human
404   lung has remained unknown. We therefore asked whether secretory cells in the human distal
405   lungs have the potential to convert into AT2 cells, governed by Notch signalling, similar to that
406   observed in the mouse lung. By combining analysis of our scRNA-seq and ATAC-seq analysis,
407   we identified a surface marker *Kdr/Flk-1* that is specifically expressed in mouse secretory cells
408   (Extended Data Fig.10a,b), which is also supported by previous studies[42,43]. Flow cytometry
409   analysis confirmed that Kdr expression specifically marks secretory cells in the mouse lung
410   (Extended Data Fig.10c-e). We then analysed recently-published scRNA-seq data[44,45] and
411   found that *KDR* is also highly expressed in secretory cells in adult human lung tissue (Extended
412   Data Fig. 10f,g). We further confirmed the expression of KDR in secretory cells of distal
413   human lung tissue by IF staining (Fig. 7a). In combination with a human AT2 cell-specific
414   surface marker HTII-280, we were able to sort KDR+HTII-280− cells by flow cytometry
415   analysis (Fig. 7b). Further analysis of cytospin staining on freshly isolated KDR−HTII-280+
416   and KDR+HTII-280− populations revealed that CC10+ secretory cells were specifically
417   enriched in the KDR+ population (Fig. 7c,d). We also confirmed that KDR+HTII-280− cells
418   showed higher expression of secretory cell markers, such as *SCGB1A1* and *SCGB3A2*, and
419   lower expression of AT2 cell markers, such as *SFTPC*, compared to KDR−HTII-280+ AT2 cells
420   (Fig. 7e). Furthermore, KDR+HTII-280− secretory cells could form organoids consisting of

421   mainly CC10$^+$ secretory cells and some Act-Tub$^+$ ciliated cells, with a few KRT5$^+$ basal cells

422   in our culture conditions (Fig. 7f, **See Method**).

423

424   Given that human secretory cells also showed higher Notch activity (e.g. *HES1* expression)

425   similar to mouse tissue (Extended Data Fig. 10f), we inhibited Notch activity by treating

426   organoids derived from KDR$^+$HTII-280$^-$ cells with DAPT to investigate the differentiation

427   potential of human secretory cells into AT2 cells. Notably, similar to mouse secretory cells,

428   Notch inhibition induced the morphological changes of human secretory cell derived-

429   organoids with significant upregulation of AT2 marker expression, such as *SFTPC*, whereas

430   the expression of secretory cell markers, including *SCGB1A1* was significantly reduced (Fig.

431   7g,h). IF staining also confirmed that Notch inhibition drives the generation of SPC$^+$ AT2 cells

432   at the expense of SCGB1A1/CC10$^+$ secretory cells in DAPT-treated organoids (Fig. 7i,j). We

433   barely observed any significant alterations in other lineages such as Act-Tub$^+$ ciliated cells and

434   KRT5$^+$basal cells (Extended Data Fig. 10h-j). Overall, our data suggest that KDR$^+$ secretory

435   cells share a conserved key molecular component of Notch signalling in governing alveolar

436   regeneration of human and mouse lungs.

Discussion

Spatiotemporal dynamics of stem and progenitor cells ensure the rapid and efficient process of tissue repair for the reconstruction of epithelial integrity and function. In response to severe lung injury, secretory cells localised in the distal airway mobilise and differentiate into AT2 cells to compensate for the loss of alveolar epithelium and restore alveolar function. However, the cellular events and regulatory networks directing the differentiation plasticity of secretory cells, and the identity of the functional niches during this process, have been largely elusive. Particularly, how secretory cells are activated and acquire differentiation plasticity is unknown. Here, our data reveal two sequential stages of secretory cell fate conversion into AT2 cells during alveolar regeneration. Loss of Notch activity mediated by IL-1β signalling in ciliated cells reprograms the secretory cells to lose their identity upon injury. Fosl2/Fra2-mediated AP-1 transcription factor then drives the fate conversion of secretory cells into AT2 cells. Furthermore, using scRNA-seq and ATAC-seq analysis, we identified that secretory-derived AT2 cells post injury retain the airway lineage identity in both a genetic and epigenetic manner, and have greater functional capacity of long-term maintenance *in vitro* compared to resident AT2 cells. By identifying a surface marker KDR/FLK-1 of human secretory cells, we propose that functionally equivalent human secretory cells are capable of contributing to alveolar lineages post injury via Notch signalling.

In this study, we uncovered the role of Notch signalling as a key regulator in reprogramming secretory cells to acquire differentiation plasticity post alveolar injury. Inhibition of Notch signalling resulted in the loss of secretory cell identity and simultaneously enhanced the fate conversion to AT2 cells upon injury. In contrast, constitutive activation of Notch signalling substantially blocked AT2 cell differentiation from secretory cells post injury, indicating that regulation of Notch activity is critical for regeneration in the context of the lung. Instead, cells were arrested at the intermediate cell state expressing high levels of *Cdkn1c/p57* expression, which is likely to link the fate transition between secretory and AT2 cells. These results reveal that the downregulation of Notch activity is indispensable for AT2 cell differentiation from secretory cells during regeneration. Notably, the intermediate population is specifically marked by the expression of *Fstl1* that has been known to antagonize BMP signalling[46]. Given the functional role of BMP signalling in facilitating proximal epithelium with a concurrent reduction in the distal epithelium during lung development[46,47], impaired alveolar regeneration in constitutive Notch activity could be connected to compromised proximal-distal patterning, which may be due to inhibition of BMP signalling. It would be interesting to further define the

15

471   presence of *Fstl1*-like populations in lung development, and whether alveolar regeneration

472   reflects the developmental stages.

473

474   How is the activity of the Notch pathway in secretory cells controlled? Given the

475   communication characteristics of Notch signalling via direct contact, we identified ciliated

476   cells as functional niches to induce Notch signalling in secretory cells by expressing Notch

477   ligands, including Jag1, which is also consistent with a previous study in the developing lung[29].

478   An increasing body of evidence is revealing that inflammation induced by tissue injury

479   modulates repair and tissue regeneration[48-50]. Indeed, our recent study showed that acute

480   inflammatory niches driven by IL-1β are essential for alveolar regeneration[30]. Of note, we

481   found that *Il1r1* is highly expressed in ciliated cells, and the expression of Notch ligands on

482   ciliated cells is regulated by IL-1β signalling. Specific deletion of *Il1r1* in ciliated cells

483   significantly impaired the contribution of secretory cells in alveolar reconstruction. This is

484   suggestive that an IL-1β-mediated inflammatory niche coordinates alveolar regeneration by

485   regulating the behaviour and cell fate transition of distal secretory cells, in addition to subsets

486   of *Il1r1*$^+$ AT2 cells post injury[30].

487

488   By combining ATAC-seq and RNA-seq analysis, we identified Fra2/Fosl2, which together

489   comprise the heterodimeric AP-1 transcription factor, as an essential driver for the fate

490   conversion of secretory cells into AT2 lineages. Notably, we found that the components of the

491   AP-1 family were differentially expressed in control and DAPT-treated organoids derived from

492   secretory cells. While the expression of *c-Jun*, *c-Fos*, *Junb*, and *Fosb* was downregulated by

493   DAPT treatment, the expression of *Fosl2* and *Jund* were specifically upregulated. Further, the

494   Harmonizome database also shows that Fosl2 is a functional target of Rbpj, a key mediator of

495   Notch signalling, and several regulatory regions of AT2 markers, including *Sftpc* and *Etv5*, are

496   directly occupied by *Fosl2*[51]. Importantly, *Fosl2*-deficient secretory cells failed to acquire AT2

497   cell differentiation in the presence of DAPT, however decreased secretory cells were not

498   recovered. Further, *Fosl2* KD didn't influence the cell fate of secretory cells without Notch

499   inhibition. These data suggest that Notch inhibition coordinates the cell fate decisions of

500   secretory cells into AT2 lineages in two stages: 1) loss of secretory cell identity and 2)

501   acquisition of transcriptional programmes for AT2 cell differentiation (Extended Data Fig.

502   10k). Our data revealed that Fosl2 is required for AT2 cell conversion from secretory cells, but

503   dispensable for the loss of secretory cell identity. Other candidates, such as *Foxc2* and *Six1*,

504   that occupy the regulatory region of secretory cell-specific genes and are substantially

16

505   downregulated by Notch inhibition (Fig.5d), could be tested for potential roles in regulating

506   the maintenance of secretory cell identity.

507

508   Notch inhibition has been reported to promote the differentiation of secretory cells into ciliated

509   cells in lung development and homeostatic adult lungs, although there are some differences in

510   the incidence of ciliated cell differentiation, potentially due to different contexts or model

511   systems[25-27]. In this study, we demonstrated that, during alveolar regeneration after injury,

512   Notch inhibition facilitated the fate conversion of secretory cells into AT2 cells via *IL-1β-*

513   *Notch-Fosl2* axis. Despite increased ciliated cell differentiation of *dnMAML*-expressing

514   secretory cells prior to injury, persistent Notch inhibition enhanced AT2 cell differentiation via

515   *Fosl2* during injury repair. How does *Fosl2* regulate this process? Interestingly, withdrawals

516   of WNT signalling-inducing factors, including Wnt3a and R-spondin-1, in our organoid

517   cultures, showed a dramatic increase in Act-Tub$^+$ ciliated cells at the expense of secretory cells

518   in DAPT-treated organoids (Extended Data Fig.10l). AT2 cells were barely observed in these

519   organoids (Extended Data Fig.10l). This result suggests that Notch and WNT signalling likely

520   function cooperatively in secretory cells differentiating to AT2 cells. Indeed, previous studies

521   showed increased expression of Wnt ligands in mesenchymal cells during alveolar regeneration

522   after injury[19,52]. Further analysis of scRNA-seq from our previous study[30] revealed that Wnt

523   ligands, such as *Wnt5a* and *Wnt7b*, were highly upregulated at day 14 and returned back to

524   homeostatic levels at day 28 post bleomycin injury (Extended Data Fig.10m). Notably,

525   however, *Fosl2*-KD secretory cells failed to generate AT2 cells even in the presence of Wnt

526   activity (Fig. 5g). Given these results, it is likely that increased Wnt ligands from mesenchymal

527   cells, in parallel with Notch-mediated Fosl2 activity, may cooperatively confer differentiation

528   potential of secretory cells into AT2 lineages, via independent regulatory axes, during alveolar

529   injury repair. While Fosl2 was identified as a key factor in the axis of Notch signalling, further

530   identification of interacting partners regulated by Wnt signalling will uncover the molecular

531   networks governing the fate decision of secretory cells into ciliated or AT2 cells in homeostasis

532   and regeneration.

533

534   Increasing evidence reveals the plasticity of epithelial stem cells under regenerative conditions.

535   In the distal lungs, two stem cell compartments, secretory cells and AT2 cells, maintain the

536   airway and alveolar epithelium, respectively, in homeostasis and regeneration. However, upon

537   severe damage, secretory cells acquire differentiation plasticity to generate alveolar lineages.

538   Interestingly, we found that sAT2 cells display distinct features compared to resident AT2

17

539   (rAT2) cells, even after injury resolution. sAT2 cells still retained some airway lineage identity
540   based on the higher expression of secretory cell markers such as *Scgb1a1* and *Sox2*, whereas
541   most genetic and epigenetic signatures of genes, including canonical AT2 cell markers such as
542   *Sftpc* and *Etv5*, are shared with rAT2 cells. Notably, sAT2 cells are capable of long-term self-
543   renewal compared to rAT2 cells in *in vitro* organoids, which may be attributed to the enriched
544   signatures of anti-apoptotic functions such as *Slc7a11* and *Nr4a2* in sAT2 cells compared to
545   rAT2 cells. sAT2 cells may have a higher tolerance for severe alveolar insults than rAT2 cells,
546   enabling them to replenish damaged alveolar epithelium more efficiently. Notably, in chronic
547   lung diseases such as pulmonary fibrosis and lung cancer, the destruction of alveolar structure
548   with bronchiolization is a common feature[53,54]. Moreover, AT2 cells expressing airway-
549   restricted genes such as Sox2 were also seen in fibrosis patients[55]. Given our findings, it would
550   be interesting to explore further whether the genetic and epigenetic memory of sAT2 cells
551   contributes to this pathologic phenotype after injury resolution.

552

553   The loss of alveolar integrity is a life-threatening and key pathologic feature of various chronic
554   lung diseases. Recent studies suggested the regenerative potential of human HTII-280^{+} AT2
555   cells using an *in vitro* organoid model, yet their capacity to generate new alveolar epithelium
556   seems limited[22,23]. In particular, the functional capacity of human airway secretory cells to
557   contribute to alveolar lineages has never been explored, largely due to the lack of information
558   for isolation and culture of secretory cells *in vitro*. Here we provide the first evidence of the
559   potential progenitor capacities of secretory cells in self-renewal and generation of AT2 cells
560   using human cells, by identifying KDR/FLK-1 as the surface marker of secretory cells and
561   establishing a feeder-free organoid culture. We furthermore demonstrated that KDR[+] secretory
562   cells in human lungs have the differentiation plasticity to give rise to AT2 cells, which is also
563   regulated by Notch signalling, as we demonstrated in mouse lungs. Our findings provide a solid
564   foundation for further studies of the potential role of these cells in chronic lung diseases.

565

566   In summary, our results identify the molecular and cellular mechanisms of the cross-
567   compartment contribution of airway secretory cells to the regeneration of the alveolar
568   epithelium after lung injury. The presence of conserved markers and ease of cultivation of both
569   mouse and human secretory cells provide a unique opportunity for mechanistic studies to shed
570   light on human lung progenitor cell biology and assist in developing new treatments for acute
571   and chronic lung diseases. Our study also provides clues for the potential therapeutic targets of
572   Notch signalling in lung diseases caused by defective and dysregulated alveolar regeneration.

Author contribution: J.C. Y.J.J, J.K., and J.-H.L. designed the experiments, interpreted the data, and wrote the manuscript; J.C. performed most experiments and data analysis; Y.J.J. performed and analysed bulk RNA-seq and ATAC-seq data; C.D. designed and performed lineage-tracing analysis of *Red2-Notch^{N1ICD}* mice, provided valuable comments on the manuscript; E. I. generated the *Sftpc-IRES-DTR-P2A-dsRed* targeting vector; K.V.E. performed the isolation of human lung tissue; J.-H.L. generated *Sftpc-IRES-DTR-P2A-dsRed* mouse line; B.-K.K. helped with the generation of the *Sftpc-IRES-DTR-P2A-dsRed* targeting vector and shared the *Red2-Notch^{N1ICD}* mice line; B.D.S helped with the study of *Red2-Notch^{N1ICD}* lineage-tracing analysis; H.H. and S.M.J provided human lung tissue samples.

Declaration of interests: The authors declare that they have no competing interests.

Data and materials availability: All open access-consented sequencing data (i.e. bulk RNA-seq, scRNA-seq, and ATAC-seq) will be deposited upon acceptance of the manuscript.

19

607 **Methods**

608 **Animals**. *Scgb1a1-CreER*[TM][13], *Sftpc-CreER*[T2][5], *Foxj1-CreER*[T2][31], *Red2-Notch*[N1ICD] (Yum et

609 al., under revision), *Rosa26R-CAG-fGFP*[13], *Rosa26R-lox-stop-lox-tdTomato*[56], and

610 *Il1r1*[flox/flox][57] mice have been described and are available from Jackson Laboratory. Il1r1-P2A-

611 eGFP-IRES-CreER[T2] (*Il1r1-CreER*[T2])[30]. To monitor SPC-expressing AT2 cells, our lab

612 generated Sftpc-IRES-DTR-P2A-dsRed (*Sftpc-dsRed*[IRES-DTR]) reporter mouse where IRES-

613 DTR-P2A-dsRed construct is inserted into 3'-UTR region of endogenous Sftpc gene. Mice for

614 the lineage tracing and injury experiments were on a C57BL/6 background and 6-10 week old

615 mice were used for most of the experiments described in this study. Experiments were

616 approved by local ethical review committees and conducted according to UK Home Office

617 project license PC7F8AE82. Mice were bred and maintained under specific-pathogen-free

618 conditions at the Cambridge Stem Cell Institute and Gurdon Institute of University of

619 Cambridge.

620

621 **Tamoxifen**. Tamoxifen (Sigma) was dissolved in Mazola corn oil (Sigma) in a 20mg/ml stock

622 solution. 0.2mg/g body weight tamoxifen was given via intraperitoneal (IP) injection. The

623 numbers and date of treatment are indicated in the individual figures of each experimental

624 scheme.

625

626 **Bleomycin administration**. 6-10 week-old mice were anesthetised via inhalation of isoflurane

627 for approximately 3 mins. The mice were positioned on the intratracheal intubation stand, and

628 1.25U/kg of bleomycin, or PBS control, were delivered intratracheally by a catheter (22G).

629 During the procedure anaesthesia was maintained by isoflurane and oxygen delivery.

630

631 **Mouse lung tissue dissociation and flow cytometry**. Lung tissues were dissociated with a

632 collagenase/dispase solution as previously described[30]. Briefly, after lungs were cleared by

633 perfusion with cold PBS through the right ventricle, 2ml of dispase (BD Biosciences, 50Uml)

634 was instilled into the lungs through the trachea until the lungs inflated. Each lobe was dissected

635 and minced into small pieces in a conical tube containing 3 ml of PBS, 60μl of

636 collagenase/dispase (Roche), and 7.5μl of 1% DNase I (Sigma) followed by rotating incubation

637 for 45 min at 37°C. The cells were then filtered sequentially through 100- and 40-μm strainers

638 and centrifuged at 1500 rpm for 5 min at 4°C. The cell pellet was resuspended in 1ml of RBC

639 lysis buffer (ACK buffer, 0.15M NH4Cl, 10mM KHCO3, 0.1mM EDTA) and lysed for 2 min

640   at room temperature. 6 ml basic F12 media (GIBCO) was added and 500µl of FBS (Hyclone)

641   was slowly added in the bottom of tube. Cells were centrifuged at 1500 rpm for 5 min at 4°C.

642   The cell pellet was resuspended in PF10 buffer (PBS with 10% FBS) for further staining. The

643   antibodies used were as follows: CD45 (30-F11)-APC or -APC-Cy7 (BD Biosciences), CD31

644   (MEC13.3)-APC (BD Biosciences), EpCAM (G8.8)-PE-Cy7 or FITC (BioLegend), and CD24

645   (M1/69)-APC (eBioscience), MHC-II (I-A/I-E, M5)-FITC or -APC-Cy7 (eBioscience), and

646   CD309/Kdr/Flk-1 (7D4-6)-APC (BioLegend). 4', 6-diamidino-2-phenylindole (DAPI) (Sigma)

647   was used to eliminate dead cells. Data were acquired on LSRII analyser (BD Bioscience) and

648   then analysed with FlowJo software (Tree Star). MOFLO system (Beckman Coulter) was used

649   for the sorting at Cambridge NIHR BRC Cell Phenotyping Hub.

650

651   **Human lung tissue dissociation and flow cytometry**. Human lung tissues were cleared by

652   perfusion with cold PBS and cut into small (1 mm) pieces. Small pieces of lung tissues (2 cm

653   x 2 cm) were moved into a conical tube containing 10 ml of digestion buffers (2ml of dispase

654   II (Sigma), 100 µl of collagenase/dispase (Roche), 100 µl of 1% DNase I (Sigma), and 7.8 ml

655   of PBS), followed by rotating incubation for 1 hr at 37 °C. The cells were then filtered through

656   100 µm strainers and centrifuged at 350 g for 5 min at 4°C. The cell pellet was resuspended in

657   5 ml of RBC lysis buffer (ACK buffer, 0.15 M NH4Cl, 10 mM KHCO3, 0.1 mM EDTA) and

658   lysed for 5 min at room temperature. 10 ml basic F12 media (GIBCO) was added and 500 µl

659   of FBS (Hyclone) was slowly added in the bottom of tube. Cells were centrifuged at 350g for

660   5 min at 4°C. The cell pellet was resuspended in PF10 buffer (PBS with 10% FBS) for further

661   staining. The antibodies used were as follows: CD45 (2D1)-APC (BioLegend), CD31 (VM59)-

662   APC (BioLegend), EpCAM (9C4)- FITC (BioLegend), HTII-280-mouse IgM (Terrace

663   Biotech), Purified CD309/KDR (A16085H), anti-mouse IgG1 (RMG1-1)-APC-Cy7

664   (BioLegend), and anti-mouse IgM (Il/41)-PE (eBioscience). 4', 6-diamidino-2-phenylindole

665   (DAPI) (Sigma) was used to eliminate dead cells. MOFLO system (Beckman Coulter) or

666   Flexible BD Influx™ cell sorter were used for the sorting at Cambridge NIHR BRC Cell

667   Phenotyping Hub and data were analysed with FlowJo software (Tree Star).

668

669   ***In vitro* feeder-free organoid culture and passages**. Freshly sorted lineage-labelled cells from

670   *Scgb1a1-CreER^{TM};R26R^{tdTomato}* or *Sftpc-CreER^{T2};R26R^{tdTomato}* mice were resuspended in basic

671   medium (AdDMEM/F12 (Invitrogen) supplemented with B27 (Invitrogen), 1mM *N*-

672   Acetylcysteine (Sigma), 10 mM Nicotinamide (Sigma)). Then, cells were mixed with growth

673   factor-reduced Matrigel (BD Biosciences) at a ratio of 1:1. A 100 µl mixture was placed in a

21

674   24-well Transwell insert with a 0.4 μm pore (Corning). Approximately 10×10^3 epithelial cells

675   were seeded in each insert. After Growth Factor Reduced Matrigel (GFR) formed a gel, 500 μl

676   of culture medium (basic medium supplemented with the growth factors: 50 ng/ml murine EGF

677   (Life Technology), 100 ng/ml human FGF7/KGF (Peprotech), 100 ng/ml human FGF10

678   (Peprotech), 50% WNT3A-conditioned media (provided by Tissue Core Facility of Cambridge

679   Stem Cell Institute), 10% RSPO1-conditioned media (provided by Tissue Core Facility of

680   Cambridge Stem Cell Institute), 100 ng/ml Noggin (Peprotech)) was placed in the lower

681   chamber. Medium was changed every other day and ROCK inhibitor Y27632 (10 μM, Sigma)

682   was added in the medium for the first 2 days of culture. Passage was performed once per 2

683   weeks at least for 12 months. For passages, organoids were removed from the Matrigel by

684   incubation with dispase (1 mg/ml) for 40 mins at 37 °C, followed by dissociation into single

685   cells using trypLE (Gibco) treatment for 5 min at 37 °C. $5 \sim 10 \times 10^3$ cells were transferred to

686   fresh Matrigel in 24-well Transwell insert. For organoid culture from a single cell with limiting

687   dilution, FACS-sorted cells were plated into 48-well plates (Corning) with one cell per well.

688   Every dilution was replicated in 48-well plates (Corning) for two independent experiments.

689   Single cells imbedded in Matrigel were monitored at microscope with RFP channels to check

690   the expression of Tomato expression.

691

692   For human KDR$^+$ cell culture in organoids, approximately 10×10^3 epithelial cells were

693   resuspended in a 20 μl of 100% GFR-Matrigel and seeded in 48 well plates, followed by 30min

694   incubation at 37 °C for solidification. Then, 250μl of airway cell culture medium (basic

695   medium supplemented with the growth factors: murine EGF (50 ng/ml, Life Technology),

696   human FGF7/KGF (100 ng/ml, Peprotech), human FGF10 (100 ng/ml, Peprotech), Noggin

697   (100 ng/ml, Peprotech), A83-01 (1 μM, Tocris), SB202190 (1 μM, Tocris) was added to each

698   well. To avoid the growth of fungal and bacterial infection, 250 ng/mL Amphotericin B and

699   50μg/mL gentamicin were added to culture medium. For culture with DATP treatment in

700   Fig.7g, organoids cultured for 8 days with airway cell culture medium were followed by

701   inclusion of CHIR99021 (2 μM, Tocris) for additional 10 days with or without DAPT (20 μM).

702   Medium was changed every 3-4 days and ROCK inhibitor Y27632 (10 μM, Sigma) was added

703   in the medium for the first 4 days of culture. Passage was performed once per 3 weeks.

704

705   **Knockdown construct and retroviral infection to organoids**. For sequence-specific

706   knockdown of candidate genes, target sequences were cloned into MSCV-LTRmiR30-PIG

707   (LMP, Open Biosystems) retroviral vectors or pLKO.1-puro lentiviral vector. To generate

22

708 retroviruses for infection into cells, the HEK293T cells were transfected using a standard

709 calcium phosphate protocol with vectors expressing GFP alone (Control-RV), GFP plus short-

710 hairpin against target genes. Viral supernatants were harvested 2 days later. Secretory-derived

711 organoids of passages between 15 and 20 were prepared after recovery from Matrigel (BD

712 Biosciences) by treatment of dispase (1mg/ml) for 40 min at 37°C, followed by dissociation

713 into single cells using trypLE (Gibco) treatment for 5 min at 37°C. Single cells dissociated

714 from established organoids were infected with the viral supernatants in the presence of

715 polybrene (Sigma, 8μg/ml) by spin infection for 90 min at 2400rpm at 32°C. This procedure

716 was repeated twice every day. Short-hairpin sequences for target genes are as follows:

717

718 fgeOshEtv5: 5'- TTCTATGAGCTTAAATTCCGC-3'

719 shCebpa: 5'-TTTGTTTGGCTTTATCTCCGC -3'

720 shSrebf2: 5'-TATTTGATGTAATCAATGCGC-3'

721 shRbpjl: 5'-TTCAAAGTTCAACTTCTGCGC-3'

722 shFosl2: 5'-TATATCTACCCGGAACTTCGC-3'

723 shRbpj: 5'-GCAGACTCATTGGGCTACATT-3'

724

725 ***In vitro* lung organoid co-culture with established stromal cells**. Freshly sorted lineage-

726 labelled cells were resuspended in culture medium (3D basic medium (DMEM/F12, Gibco)

727 supplemented with 10% FBS. (Gibco) and ITS (Insulin-Transferrin-Selenium, Corning)), and

728 mixed with cultured lung stromal cells negatively isolated by microbeads of CD326/EpCAM,

729 CD45, and CD31 via MACS (Miltenyi Biotech), followed by resuspension in growth factor-

730 reduced Matrigel (BD Biosciences) at a ratio of 1:5. A 100 μl mixture was placed in a 24-well

731 Transwell insert with a 0.4 μm pore (Corning). Approximately 5×10^3 epithelial cells were

732 seeded in each insert. 500 μl of culture medium was placed in the lower chamber, and medium

733 was changed every other day. ROCK inhibitor Y27632 (10 μM, Sigma) was added in the

734 medium for the first 2 days of culture. Analysis of colony forming efficiency (CFE) and size

735 of organoids was performed at 14 days after plating if there is no specific description.

736

737 ***In vitro* culture of ciliated cells for IL-1β treatment.** CD24^{high}Tomato^{+} ciliated cells were

738 isolated from *Il1r1-CreER^T2* mice at day 4 after four doses of tamoxifen treatment. Purified

739 20,000 cells were embedded in Matrigel with PBS or IL-1β (10 ng/ml) for 24 hrs. Then, RNA

740 was isolated to analyse the expression of *Jag1* or *Jag2*.

741

742 **Transplantation of *Scgb1a1*⁺ lineage-labelled cells**. Freshly sorted 20,000 cells of

743 CD45^{−}EpCAM⁺Tomato⁺MHCII^{−} cells from *Scgb1a1-CreER^{TM/+};R26R^{tdTomato/+}* or

744 *dnMAML^{flox/+};Scgb1a1-CreER^{TM/+};R26R^{tdTomato/+}* mice were mixed with lung stromal cells

745 isolated from WT mice (20,000 cells) to support epithelial cell survival during engraftment,

746 and were transplanted into WT C57BL/6 mice at day 7 after bleomycin injury (1.25 U/kg).

747 Lungs were analysed at day 14 post injury to determine the differentiation of engrafted cells.

748

749 **Quantitative RT-PCR.** Total RNA was isolated using a Qiagen RNeasy Mini-plus Kit

750 according the manufacturer's instructions. Equivalent quantities of total RNA were reverse-

751 transcribed with SuperScript IV cDNA synthesis kit (Life Technology). Diluted cDNA was

752 analysed by real-time PCR (StepOnePlus; Applied Biosystem). Pre-designed probe sets

753 (Thermo Fisher Scientific) were used as follows: human Scgb1a1 (Hs00171092_m1), human

754 Sftpc (Hs00951326_g1), and Human Foxj1 (Hs00230964_m1). Actb expression

755 (Hs01060665_g1) was used to normalise samples using the ΔCt method. Sybr green assays

756 were also used for human or mouse gene expression with SYBR Green Master Mix (2x,

757 Thermo Fisher Scientific). Primer sequences are as follows:

758

759 Mouse:

760 Gapdh: F-AGGTCGGTGTGAACGGATTTG, R-TGTAGACCATGTAGTTGAGGTCA

761 Scgb1a1: F- ATGAAGATCGCCATCACAATCAC, R-GGATGCCACATAACCAGACTCT

762 Scgb3a2: F-CCACTGCCCTTCTCATCAACC, R-TGTCGTCCAAAGGTACAGGTA

763 Gabrp: F-CAGACCCACGGCTAGTGTTC, R- AGAGGCGGATGAGCCTGTT

764 Cldn10: F-AATCGTCGCCTTCGTAGTC, R-GTTGGCAAAAATAAGTGGCT

765 Cyp2f2: F- GGACCCAAACCTCTCCCAATC, R- CCGTGAACACCGACCCATAC

766 Sftpc: F-TCAGTCTGATAACTTGGTGCTTC, R-GGCTTCCTATCGTAGGCACAA

767 Etv5: F-TCAGTCTGATAACTTGGTGCTTC, R-GGCTTCCTATCGTAGGCACAA

768 Lamp3: F- TCCAAAAGCCAGAGGCTATCT, R- ACTGGGGTTACTGTTTTCATTGT

769 Lpcat1: F-GGCTCCTGTTCGCTGCTTT, R-TTCACAGCTACACGGTGGAAG

770 Abca3: F-CAGCTCACCCTCCTACTCTG, R-ACTGGATCTTCAAGCGAAGCC

771 Jag1: F-CCTCGGGGTCAGTTTGAGCTG, R-CCTTGAGGCACACTTTGAAGTA

772 Jag2: F-CAATGACACCACTCCAGATGAG, R-GGCCAAAGAAGTCGTTGCG

773 Dll-1: F- CAGGACCTTCTTTCGCGTATG, R- AAGGGGAATCGGATGGGGTT

774 Dll-4: F- TTCCAGGCAACCTTCTCCGA, R- ACTGCCGCTATTCTTGTCCC

24

775   Hes1: F-CCAGCCAGTGTCAACACGA, R-AATGCCGGGAGCTATCTTTCT

776   Nrarp: F-TTCAACGTGAACTCGTTCGGG, R-TTGCCGTCGATGACTGACTG

777

778   Human:

779   Scgb3a2: F- AAGCTGGTAACTATCTTCCTGCT, R- AGGGGCACTTTGTTGATGAGG

780   Lamp3: F- ACTACCCCAGCGACTACAAAA, R- CTAGGGCCGACTGTAACTTCA

781   Etv5: F- TCAGCAAGTCCCTTTTATGGTC, R- GCTCTTCAGAATCGTGAGCCA

782

783   **Cytospin, Immunofluorescence, and immunohistochemistry**. Mouse lung tissues were

784   routinely perfused, inflated, and fixed with 4% PFA for 2 hrs at 4°C. Cryosections (8-12μm)

785   and paraffin sections (7μm) were used for histology and Immunofluorescence (IF) analysis.

786   Cultured colonies from organoids were fixed with 4% PFA for 2 hrs at room temperature

787   followed by immobilisation with Histogel (Thermo Scientific) for paraffin embedding. For

788   cytospin staining, isolated 2,000 cells were resuspended in 250μl of PBS supplemented with

789   10% FBS, followed by spinning in pre-wet cytospin funnels at 600rpm for 5min. Sectioned

790   lung tissues or colonies were stained with hematoxylin and eosin (H&E) or immunostained:

791   after antigen retrieval with citric acid (0.01M, pH 6.0), blocking was performed with 5%

792   normal donkey serum in 0.2% Triton-X/PBS at room temperature for 1hr. Primary antibodies

793   were incubated overnight at 4°C at the indicated dilutions: Goat anti-CCSP/CC10 (T-18)

794   (1:200, Santa Cruz Biotechnology Inc., sc-9772), Mouse anti-CCSP/CC10 (E11) (1:200, Santa

795   Cruz Biotechnology Inc., sc-365992), Goat anti-SP-C (1:200, Santa Cruz Biotechnology Inc.,

796   sc-7706), Rabbit anti-pro-SP-C (1:300, Millipore, AB3786), Mouse anti-Acetylated Tubulin

797   (6-11B-1) (1:300, Sigma-Aldrich, T7451), Hamster anti-PDPN (1:300, DSHB, 8.1.1), Rabbit

798   anti-KRT5 (1:300, BioLegend, 905501), Mouse anti-P63 (1:200, Abcam, ab735), Rabbit anti-

799   PORCN (1:100, Abcam, ab201793), Rabbit anti-P57/KIP2 (1:100, Abcam, ab75974), Rabbit

800   anti-RFP (1:250, Rockland, 600–401379), Rabbit anti-HOPX (1:100, Santa Cruz

801   Biotechnology Inc., sc-30216), Rabbit anti-HES1 (1:200, D6P2U, #11988, Cell Signaling),

802   Rabbit anti-NOTCH1 (1:50, Abcam, ab52627), Mouse IgM anti-HT2-280 (1:300, Terrace

803   Biotech, TB-27AHT2-280), Rat anti-human SCGB1A1/CC10 (1:200, R&D system,

804   MAB4218), Rabbit anti-KDR/VEGFR2 (1:100, Cell Signaling, 2479). Alexa Fluor-coupled

805   secondary antibodies (1:500, Invitrogen) were incubated at room temperature for 60 min. After

806   antibody staining, nuclei were stained with DAPI (1:1000, Sigma) and sections were embedded

807   in RapiClear® (SUNJin Lab). Fluorescence images were acquired using a confocal microscope

808   (Leica TCS SP5). All the images were further processed with Fiji software. For

25

809   immunohistochemical staining of Jag1 was done by using Anti-human Jag1 antibody (1:100,

810   Santa Cruz Biotechnology Inc., sc-390177). Slides were developed by using mouse IgG

811   VECTASTAIN Elite ABC kit (Vector Laboratories). Slides were counterstained with

812   haematoxylin.

813

814   **Statistical analysis**. Statistical methods relevant to each figure are outlined in the figure legend.

815   Statistical analyses were performed with Prism software package version 7.0

816   (GraphPad). P values were calculated using two-tailed unpaired Student's t test or Two-way

817   ANOVA for multiple group comparison (Fig. 2i, and 4b,e). Sample size for animal experiments

818   was determined based upon pilot experiments. Mice cohort size was designed to be sufficient

819   to enable accurate determination of statistical significance. No animals were excluded from the

820   statistical analysis. Mice were randomly assigned to treatment or control groups, while

821   ensuring inclusion criteria based on gender and age. Animal studies were not performed in a

822   blinded fashion. The number of animals shown in each figure is indicated in the legends

823   as $n = x$ mice per group. Data shown are either representative of three or more independent

824   experiments, or combined from three or more independent experiments as noted and analysed

825   as mean ± s.e.m.

826

827   **Cell counting and image analysis.** Sections included in cell scoring analysis for lung tissue

828   were acquired using Leica TCS SP5 confocal microscope. At least six different sections under

829   10X magnification including at least 9 different alveolar regions from individual mice indicated

830   in the figures per group were used. Cell counts were performed on ImageJ using the 'Cell

831   Counter' plug-in and the performer was blinded to the specimen genotype and condition. At

832   least two step sections (30μm apart) per individual well were used for quantification of

833   organoids.

834

835   **RNA-sequencing analysis**. RNA-seq were performed for global gene expression profiles in

836   ACOs, and SCOs with or without DAPT treatment. Total RNAs were extracted using the

837   RNeasy Plus Mini Kit following the manufacturer's instructions. 100 ng of total RNA was used

838   to generate RNA-seq library using NEBNext Ultra RNA Library prep kit (NEB, E7530L)

839   according to the vendor's protocol. Briefly, mRNAs were purified from total RNAs with

840   Magnetic mRNA Isolation Kit (oligo(dT) beads) and fragmented. First and second strand

841   cDNAs were synthesized subsequently. The double strand cDNAs were purified, and then the

842   ends of cDNAs were repaired and ligated with sample-specific barcodes. RNA-seq libraries

26

843   were sequenced using an Illumina NextSeq 500 machine. Single-ends reads from RNA-seq

844   were aligned to the reference mouse genome (mm10) using STAR (v2.5.2b). The python

845   package HTSeq (https://htseq.readthedocs.io/en/master/) was used to generate read counts for

846   each gene. The read counts were analysed by the R package DESeq2 (v1.28.0)[58] and

847   regularized log transformed using the rlog function. Adjusted p-values (p.adj) for DEG were

848   determined by Benjamini and Hochberg correction. The p.adj < 0.01 required to consider

849   differentially expressed genes. Heat maps were generated using Java Treeview (v1.1.6r4).

850

851   **ATAC-sequencing analysis.** The ATAC-seq assay was performed in two biological replicates

852   for each sample of 50,000 FACS-purified cells. The quality of data from ATAC-seq was tested

853   using FASTQC. The adapter sequences were contained in raw data. Therefore, NGmerge[59] was

854   used for adapter trimming. 150 bp paired-ends adapter trimmed reads were aligned against the

855   mouse genome assembly (mm10) using bowtie2 (v2.3.4.1). We performed peak calling using

856   MACS2 (v2.1.2) with default parameters for paired ends. Statistically significant differential

857   open chromatin regions were determined using MAnorm (v1.1.4)[60], which normalises read

858   density levels and calculates p-values by MA plot methods. The heat maps and the Spearman

859   correlation map of ATAC-seq signals were generated using deepTool2[61]. Genome browser

860   images were generated using the Integrative Genomics Viewer (IGV) 2.7.2[62] with bedGraph

861   files processed from MACS2.

862   The ATAC-seq peaks were mapped to the region surrounding 20 Kb up- and 2 Kb down-stream

863   of the TSS of all genes from refFlat file (mm10, UCSC). All assigned genomic features from

864   one open region were used. To describe the distribution of genes, a promoter was defined as a

865   region within 2 Kb from the TSS, a proximal promoter region was defined as a region between

866   2 Kb and 20 Kb upstream from the TSS. Mapping sites other than promoter, proximal promoter,

867   exon, or intron were considered as intergenic target loci. To identify the cell-type specific

868   enriched motifs in the differential open chromatin regions from ATAC-seq data, we performed

869   motif enrichment analysis using the findMotifsGenome.pl program in the HOMER software

870   (v4.11)[63]. The regions were adjusted to the same size with 200 bp centred on each differential

871   peak.

872

873   **Gene ontology (GO) analysis**. The gene ontology (GO) term enrichment analysis was

874   performed using GREAT (v4.0.4)[64] with mouse genome assembly (mm10), and whole

875   genomes for background regions in default setting from ATAC-seq data. Gene Ontology

876   tool[65,66] was used for a set of gene target of the differential open regions.

877

878 **Gene set enrichment analysis (GSEA)**. GSEA was carried out by using the Gene Ontology
879 term gene sets provided by the Mouse Genome Informatics website
880 (http://www.informatics.jax.org)[67]. Entire detectable genes derived from RNA-seq were used
881 for GSEA. We followed the standard GSEA user guide
882 (http://www.broadinstitute.org/gsea/doc/GSEAUserGuideFrame.html).

883

884 **scRNA-seq library preparation and sequencing**. For lineage-labeled cells from *Red2-*
885 *Notch^{N1ICD}* mice, YFP$^+$CD45$^-$CD31$^-$EpCAM$^+$ or RFP$^+$CD45$^-$CD31$^-$EpCAM$^+$ cells were
886 sorted at day 28 post bleomycin injury (4 mice were pooled for each experiment). For non-
887 lineage-labeled cells isolated from *Red2-Notch^{N1ICD}* mice in parallel with experiment of
888 lineage-labeled cells, we combined the cells of EpCAM$^+$RFP$^-$RFP$^-$ and EpCAM$^-$ population
889 with a ratio of 1:1, respectively. The resulting cell suspension (~110,000 cells each) were
890 submitted as separate samples to be barcoded for the droplet-encapsulation single-cell RNA-
891 seq experiments using the Chromium Controller (10X Genomics). Single cell cDNA synthesis,
892 amplification, and sequencing libraries preparation were performed using the Single Cell 3'
893 Reagent Kit as per the 10x Genomics protocol. Libraries were multiplexed so that 2 libraries
894 were sequenced per single lane of HiSeq 4000 using the following parameters: Read1: 27
895 cycles, i7: 9 cycles, i5: 0 cycles; Read2: 100 cycles to generate 150bp paired end reads.

896

897 **Data Availability**. The datasets of RNA-seq, ATAC-seq, and scRNA-seq analysis generated
898 during this study are available at GEO: GSE153677 (RNA-seq and ATACC-seq for organoids)
899 and GSE154218 (scRNA-seq). Software used to analyse the data are either freely or
900 commercially available.

901

902 **Alignment, quantification and quality control of scRNA-seq data.** Droplet-based
903 sequencing data were aligned and quantified using the Cell Ranger Single-Cell Software Suite
904 (version 2.0.2, 10x Genomics Inc) using the *Mus musculus* genome (GRCm38) (official Cell
905 Ranger reference, version 1.2.0). Cells were filtered by custom cutoff (more than 500 and less
906 than 7000 detected genes, more than 2000 UMI count) to remove potential empty droplets and
907 doublets. Downstream analysis included data normalisation, highly variable gene detection,
908 log transformation, principal component analysis, neighbourhood graph generation and
909 Louvain graph-based clustering, which was done by python package scanpy (version 1.3.6)[68]
910 using default parameters.

28

911

912 **Doublet exclusion**. To exclude doublets from single-cell RNA sequencing data, we applied

913 scrublet algorithm per sample to calculate scrublet-predicted doublet score per cell with

914 following parameters: sim_doublet_ratio = 2; n_neighbours=; expected_doublet_rate= 0.1.

915 Any cell with scrublet score > 0.7 was flagged as doublet. To propagate the doublet detection

916 into potential false-negatives from scrublet analysis, we over-clustered the dataset

917 (*sc.tl.louvain* function from scanpy package version 1.3.4; resolution = 20), and calculated the

918 average doublet score within each cluster. Any cluster with averaged scrublet score > 0.6 was

919 flagged as a doublet cluster. All remaining cell clusters were further examined to detect

920 potential false-negatives from scrublet analysis according to the following criteria: (1)

921 expression of marker genes from two distinct cell types which are unlikely according to prior

922 knowledge, (2) higher number of UMI counts.

923

924 **References**

925 1   Fuchs, E., Tumbar, T. & Guasch, G. Socializing with the neighbors: stem cells and
926   their niche. *Cell* **116**, 769-778, doi:10.1016/s0092-8674(04)00255-7 (2004).

927 2   Blanpain, C. & Fuchs, E. Stem cell plasticity. Plasticity of epithelial stem cells in
928   tissue regeneration. *Science* **344**, 1242281, doi:10.1126/science.1242281 (2014).

929 3   Butler, J. P. *et al.* Evidence for adult lung growth in humans. *N Engl J Med* **367**, 244-
930   247, doi:10.1056/NEJMoa1203983 (2012).

931 4   Hogan, B. L. *et al.* Repair and regeneration of the respiratory system: complexity,
932   plasticity, and mechanisms of lung stem cell function. *Cell Stem Cell* **15**, 123-138,
933   doi:10.1016/j.stem.2014.07.012 (2014).

934 5   Barkauskas, C. E. *et al.* Type 2 alveolar cells are stem cells in adult lung. *J Clin Invest*
935   **123**, 3025-3036, doi:10.1172/JCI68782 (2013).

936 6   Rock, J. R. *et al.* Multiple stromal populations contribute to pulmonary fibrosis
937   without evidence for epithelial to mesenchymal transition. *Proc Natl Acad Sci U S A*
938   **108**, E1475-1483, doi:10.1073/pnas.1117988108 (2011).

939 7   Adamson, I. Y. & Bowden, D. H. The type 2 cell as progenitor of alveolar epithelial
940   regeneration. A cytodynamic study in mice after exposure to oxygen. *Lab Invest* **30**,
941   35-42 (1974).

942 8   Kathiriya, J. J., Brumwell, A. N., Jackson, J. R., Tang, X. & Chapman, H. A. Distinct
943   Airway Epithelial Stem Cells Hide among Club Cells but Mobilize to Promote
944   Alveolar Regeneration. *Cell Stem Cell* **26**, 346-358 e344,
945   doi:10.1016/j.stem.2019.12.014 (2020).

946 9   Vaughan, A. E. *et al.* Lineage-negative progenitors mobilize to regenerate lung
947   epithelium after major injury. *Nature* **517**, 621-625, doi:10.1038/nature14112 (2015).

948 10   Salwig, I. *et al.* Bronchioalveolar stem cells are a main source for regeneration of
949   distal lung epithelia in vivo. *EMBO J* **38**, doi:10.15252/embj.2019102099 (2019).

950 11   Liu, Q. *et al.* Lung regeneration by multipotent stem cells residing at the
951   bronchioalveolar-duct junction. *Nat Genet* **51**, 728-738, doi:10.1038/s41588-019-
952   0346-6 (2019).

953 12   Guha, A., Deshpande, A., Jain, A., Sebastiani, P. & Cardoso, W. V. Uroplakin 3a(+)
954   Cells Are a Distinctive Population of Epithelial Progenitors that Contribute to Airway
955   Maintenance and Post-injury Repair. *Cell Rep* **19**, 246-254,
956   doi:10.1016/j.celrep.2017.03.051 (2017).

957   13   Rawlins, E. L. *et al.* The role of Scgb1a1+ Clara cells in the long-term maintenance
958   and repair of lung airway, but not alveolar, epithelium. *Cell Stem Cell* **4**, 525-534,
959   doi:10.1016/j.stem.2009.04.002 (2009).

960   14   Miller, A. J. *et al.* Generation of lung organoids from human pluripotent stem cells in
961   vitro. *Nat Protoc* **14**, 518-540, doi:10.1038/s41596-018-0104-8 (2019).

962   15   Huch, M. *et al.* Unlimited in vitro expansion of adult bi-potent pancreas progenitors
963   through the Lgr5/R-spondin axis. *EMBO J* **32**, 2708-2721,
964   doi:10.1038/emboj.2013.204 (2013).

965   16   Huch, M. *et al.* In vitro expansion of single Lgr5+ liver stem cells induced by Wnt-
966   driven regeneration. *Nature* **494**, 247-250, doi:10.1038/nature11826 (2013).

967   17   Nikolic, M. Z. *et al.* Human embryonic lung epithelial tips are multipotent progenitors
968   that can be expanded in vitro as long-term self-renewing organoids. *Elife* **6**,
969   doi:10.7554/eLife.26575 (2017).

970   18   Sachs, N. *et al.* Long-term expanding human airway organoids for disease modeling.
971   *EMBO J* **38**, doi:10.15252/embj.2018100300 (2019).

972   19   Lee, J. H. *et al.* Anatomically and Functionally Distinct Lung Mesenchymal
973   Populations Marked by Lgr5 and Lgr6. *Cell* **170**, 1149-1163 e1112,
974   doi:10.1016/j.cell.2017.07.028 (2017).

975   20   Shiraishi, K. *et al.* In vitro expansion of endogenous human alveolar epithelial type II
976   cells in fibroblast-free spheroid culture. *Biochem Biophys Res Commun* **515**, 579-585,
977   doi:10.1016/j.bbrc.2019.05.187 (2019).

978   21   Weiner, A. I. *et al.* Mesenchyme-free expansion and transplantation of adult alveolar
979   progenitor cells: steps toward cell-based regenerative therapies. *NPJ Regen Med* **4**,
980   17, doi:10.1038/s41536-019-0080-9 (2019).

981   22   Katsura, H. *et al.* Human Lung Stem Cell-Based Alveolospheres Provide Insights into
982   SARS-CoV-2-Mediated Interferon Responses and Pneumocyte Dysfunction. *Cell*
983   *Stem Cell* **27**, 890-904 e898, doi:10.1016/j.stem.2020.10.005 (2020).

984   23   Youk, J. *et al.* Three-Dimensional Human Alveolar Stem Cell Culture Models Reveal
985   Infection Response to SARS-CoV-2. *Cell Stem Cell* **27**, 905-919 e910,
986   doi:10.1016/j.stem.2020.10.004 (2020).

987   24   Maillard, I. *et al.* The requirement for Notch signaling at the beta-selection checkpoint
988   in vivo is absolute and independent of the pre-T cell receptor. *J Exp Med* **203**, 2239-
989   2245, doi:10.1084/jem.20061020 (2006).

990 25   Pardo-Saganta, A. *et al.* Parent stem cells can serve as niches for their daughter cells.
991   *Nature* **523**, 597-601, doi:10.1038/nature14553 (2015).
992 26   Lafkas, D. *et al.* Therapeutic antibodies reveal Notch control of transdifferentiation in
993   the adult lung. *Nature* **528**, 127-131, doi:10.1038/nature15715 (2015).
994 27   Morimoto, M. *et al.* Canonical Notch signaling in the developing lung is required for
995   determination of arterial smooth muscle cells and selection of Clara versus ciliated
996   cell fate. *J Cell Sci* **123**, 213-224, doi:10.1242/jcs.058669 (2010).
997 28   You, P. *et al.* Jagged-1-HES-1 signaling inhibits the differentiation of TH17 cells via
998   ROR gammat. *J Biol Regul Homeost Agents* **27**, 79-93 (2013).
999 29   Tsao, P. N. *et al.* Notch signaling controls the balance of ciliated and secretory cell
1000   fates in developing airways. *Development* **136**, 2297-2307, doi:10.1242/dev.034884
1001   (2009).
1002 30   Choi, J. *et al.* Inflammatory Signals Induce AT2 Cell-Derived Damage-Associated
1003   Transient Progenitors that Mediate Alveolar Regeneration. *Cell Stem Cell* **27**, 366-
1004   382 e367, doi:10.1016/j.stem.2020.06.020 (2020).
1005 31   Rawlins, E. L., Ostrowski, L. E., Randell, S. H. & Hogan, B. L. Lung development
1006   and repair: contribution of the ciliated lineage. *Proc Natl Acad Sci U S A* **104**, 410-
1007   417, doi:10.1073/pnas.0610770104 (2007).
1008 32   Kotton, D. N. & Morrisey, E. E. Lung regeneration: mechanisms, applications and
1009   emerging stem cell populations. *Nat Med* **20**, 822-832, doi:10.1038/nm.3642 (2014).
1010 33   Kimura, S. *et al.* The T/ebp null mouse: thyroid-specific enhancer-binding protein is
1011   essential for the organogenesis of the thyroid, lung, ventral forebrain, and pituitary.
1012   *Genes Dev* **10**, 60-69, doi:10.1101/gad.10.1.60 (1996).
1013 34   Martis, P. C. *et al.* C/EBPalpha is required for lung maturation at birth. *Development*
1014   **133**, 1155-1164, doi:10.1242/dev.02273 (2006).
1015 35   Zhang, Z. *et al.* Transcription factor Etv5 is essential for the maintenance of alveolar
1016   type II cells. *Proc Natl Acad Sci U S A* **114**, 3903-3908,
1017   doi:10.1073/pnas.1621177114 (2017).
1018 36   Didon, L., Roos, A. B., Elmberger, G. P., Gonzalez, F. J. & Nord, M. Lung-specific
1019   inactivation of CCAAT/enhancer binding protein alpha causes a pathological pattern
1020   characteristic of COPD. *Eur Respir J* **35**, 186-197, doi:10.1183/09031936.00185008
1021   (2010).

32

1022   37   Holla, V. R., Mann, J. R., Shi, Q. & DuBois, R. N. Prostaglandin E2 regulates the
1023   nuclear receptor NR4A2 in colorectal cancer. *J Biol Chem* **281**, 2676-2682,
1024   doi:10.1074/jbc.M507752200 (2006).

1025   38   Ke, N. *et al.* Nuclear hormone receptor NR4A2 is involved in cell transformation and
1026   apoptosis. *Cancer Res* **64**, 8208-8212, doi:10.1158/0008-5472.CAN-04-2134 (2004).

1027   39   Koppula, P., Zhang, Y., Zhuang, L. & Gan, B. Amino acid transporter SLC7A11/xCT
1028   at the crossroads of regulating redox homeostasis and nutrient dependency of cancer.
1029   *Cancer Commun (Lond)* **38**, 12, doi:10.1186/s40880-018-0288-x (2018).

1030   40   Dixon, S. J. *et al.* Ferroptosis: an iron-dependent form of nonapoptotic cell death. *Cell*
1031   **149**, 1060-1072, doi:10.1016/j.cell.2012.03.042 (2012).

1032   41   Lee, J. H. *et al.* Lung stem cell differentiation in mice directed by endothelial cells via
1033   a BMP4-NFATc1-thrombospondin-1 axis. *Cell* **156**, 440-455,
1034   doi:10.1016/j.cell.2013.12.039 (2014).

1035   42   Chen, H. *et al.* Airway epithelial progenitors are region specific and show differential
1036   responses to bleomycin-induced lung injury. *Stem Cells* **30**, 1948-1960,
1037   doi:10.1002/stem.1150 (2012).

1038   43   Chernaya, O., Shinin, V., Liu, Y. & Minshall, R. D. Behavioral heterogeneity of adult
1039   mouse lung epithelial progenitor cells. *Stem Cells Dev* **23**, 2744-2757,
1040   doi:10.1089/scd.2013.0631 (2014).

1041   44   Habermann, A. C. *et al.* Single-cell RNA sequencing reveals profibrotic roles of
1042   distinct epithelial and mesenchymal lineages in pulmonary fibrosis. *Sci Adv* **6**,
1043   eaba1972, doi:10.1126/sciadv.aba1972 (2020).

1044   45   Travaglini, K. J. *et al.* A molecular cell atlas of the human lung from single-cell RNA
1045   sequencing. *Nature* **587**, 619-625, doi:10.1038/s41586-020-2922-4 (2020).

1046   46   Geng, Y. *et al.* Follistatin-like 1 (Fstl1) is a bone morphogenetic protein (BMP) 4
1047   signaling antagonist in controlling mouse lung development. *Proc Natl Acad Sci U S*
1048   *A* **108**, 7058-7063, doi:10.1073/pnas.1007293108 (2011).

1049   47   Weaver, M., Yingling, J. M., Dunn, N. R., Bellusci, S. & Hogan, B. L. Bmp signaling
1050   regulates proximal-distal differentiation of endoderm in mouse lung development.
1051   *Development* **126**, 4005-4015 (1999).

1052   48   Eming, S. A., Wynn, T. A. & Martin, P. Inflammation and metabolism in tissue repair
1053   and regeneration. *Science* **356**, 1026-1030, doi:10.1126/science.aam7928 (2017).

1054   49   Naik, S. *et al.* Inflammatory memory sensitizes skin epithelial stem cells to tissue
1055   damage. *Nature* **550**, 475-480, doi:10.1038/nature24271 (2017).

1056   50   Karin, M. & Clevers, H. Reparative inflammation takes charge of tissue regeneration.
1057   *Nature* **529**, 307-315, doi:10.1038/nature17039 (2016).

1058   51   Rouillard, A. D. *et al.* The harmonizome: a collection of processed datasets gathered
1059   to serve and mine knowledge about genes and proteins. *Database (Oxford)* **2016**,
1060   doi:10.1093/database/baw100 (2016).

1061   52   Zepp, J. A. *et al.* Distinct Mesenchymal Lineages and Niches Promote Epithelial Self-
1062   Renewal and Myofibrogenesis in the Lung. *Cell* **170**, 1134-1148 e1110,
1063   doi:10.1016/j.cell.2017.07.034 (2017).

1064   53   Chilosi, M. *et al.* Aberrant Wnt/beta-catenin pathway activation in idiopathic
1065   pulmonary fibrosis. *Am J Pathol* **162**, 1495-1502, doi:10.1016/s0002-9440(10)64282-
1066   4 (2003).

1067   54   Jensen-Taubman, S. M., Steinberg, S. M. & Linnoila, R. I. Bronchiolization of the
1068   alveoli in lung cancer: pathology, patterns of differentiation and oncogene expression.
1069   *Int J Cancer* **75**, 489-496, doi:10.1002/(sici)1097-0215(19980209)75:4<489::aid-
1070   ijc1>3.0.co;2-p (1998).

1071   55   Xu, Y. *et al.* Single-cell RNA sequencing identifies diverse roles of epithelial cells in
1072   idiopathic pulmonary fibrosis. *JCI Insight* **1**, e90558, doi:10.1172/jci.insight.90558
1073   (2016).

1074   56   Madisen, L. *et al.* A robust and high-throughput Cre reporting and characterization
1075   system for the whole mouse brain. *Nat Neurosci* **13**, 133-140, doi:10.1038/nn.2467
1076   (2010).

1077   57   Robson, M. J. *et al.* Generation and Characterization of Mice Expressing a
1078   Conditional Allele of the Interleukin-1 Receptor Type 1. *PLoS One* **11**, e0150068,
1079   doi:10.1371/journal.pone.0150068 (2016).

1080   58   Love, M. I., Huber, W. & Anders, S. Moderated estimation of fold change and
1081   dispersion for RNA-seq data with DESeq2. *Genome Biol* **15**, 550,
1082   doi:10.1186/s13059-014-0550-8 (2014).

1083   59   Gaspar, J. M. NGmerge: merging paired-end reads via novel empirically-derived
1084   models of sequencing errors. *BMC bioinformatics* **19**, 1-9 (2018).

1085   60   Shao, Z., Zhang, Y., Yuan, G. C., Orkin, S. H. & Waxman, D. J. MAnorm: a robust
1086   model for quantitative comparison of ChIP-Seq data sets. *Genome Biol* **13**, R16,
1087   doi:10.1186/gb-2012-13-3-r16 (2012).

1088   61   Ramirez, F. *et al.* deepTools2: a next generation web server for deep-sequencing data
1089   analysis. *Nucleic Acids Res* **44**, W160-165, doi:10.1093/nar/gkw257 (2016).

1090   62   Thorvaldsdóttir, H., Robinson, J. T. & Mesirov, J. P. Integrative Genomics Viewer
1091   (IGV): high-performance genomics data visualization and exploration. *Briefings in*
1092   *bioinformatics* **14**, 178-192 (2013).
1093   63   Heinz, S. *et al.* Simple combinations of lineage-determining transcription factors
1094   prime cis-regulatory elements required for macrophage and B cell identities.
1095   *Molecular cell* **38**, 576-589 (2010).
1096   64   McLean, C. Y. *et al.* GREAT improves functional interpretation of cis-regulatory
1097   regions. *Nature biotechnology* **28**, 495 (2010).
1098   65   Ashburner, M. *et al.* Gene ontology: tool for the unification of biology. *Nature*
1099   *genetics* **25**, 25-29 (2000).
1100   66   Consortium, G. O. The gene ontology resource: 20 years and still GOing strong.
1101   *Nucleic acids research* **47**, D330-D338 (2019).
1102   67   Bult, C. J. *et al.* Mouse Genome Database (MGD) 2019. *Nucleic Acids Res* **47**, D801-
1103   D806, doi:10.1093/nar/gky1056 (2019).
1104   68   Wolf, F. A., Angerer, P. & Theis, F. J. SCANPY: large-scale single-cell gene
1105   expression data analysis. *Genome Biol* **19**, 15, doi:10.1186/s13059-017-1382-0
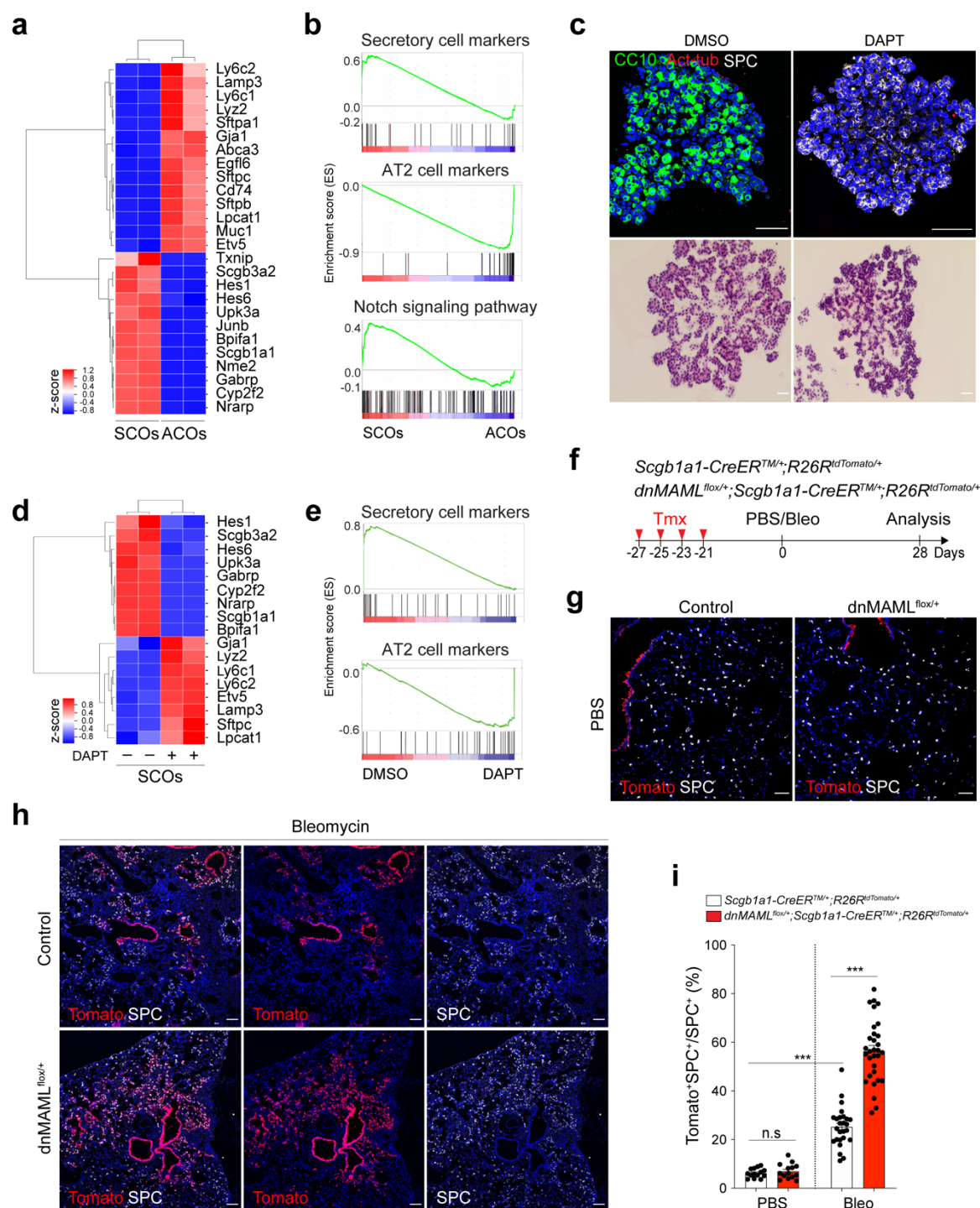1106   (2018).
1107

1108   **Figure Legends**
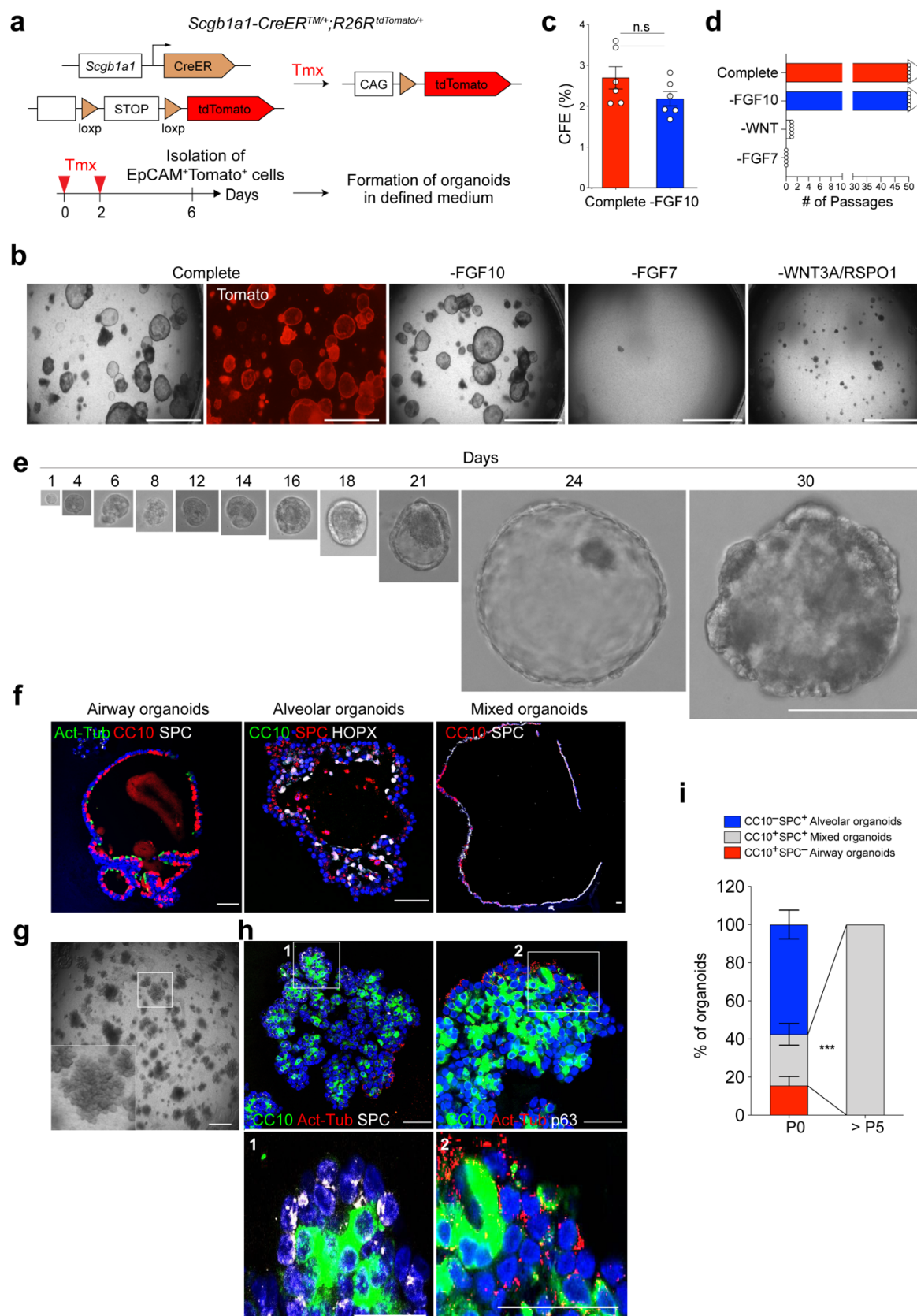
1109

1110   **Figure 1. Establishment of feeder-free organoids derived from distal secretory cells.**

a, Experimental design for isolation of *Scgb1a1* lineage-labelled cells. *Scgb1a1* lineage-labelled cells were isolated at day 4 after final tamoxifen treatment. **b,** Representative bright-field or fluorescent images of organoids derived from lineage-labelled *Tomato*$^+$*Scgb1a1*$^+$ cells in indicated conditions; complete medium (See **Methods**) with WNT3A, RSPO1 (R-spondin 1), EGF, FGF7, FGF10, and NOG (Noggin), withdrawal of indicated factors (−FGF10, −FGF7, or −WNT3A/RSPO1). Scale bar, 2,000μm. **c, d,** Statistical quantification of colony forming efficiency (**c**) and passaging numbers (**d**) of organoids. Each individual dot represents one biological replicate and data are presented as mean and s.e.m. n.s; not significant. **e,** Representative serial bright-field images of a lung organoid growing originated from single *Tomato*$^+$*Scgb1a1*$^+$ cells at the indicated time points. Magnifications: X20 (day 0 and 4), X10 (day4-21), and X4 (day 24 and 30). Scale bars, 200μm. **f,** Representative immunofluorescence (IF) images of three distinctive types of organoids derived from *Tomato*$^+$*Scgb1a1*$^+$ cells at the establishment under feeder-free condition with complete culture medium; Airway organoids retaining CC10$^+$ secretory and Act-Tub$^+$ ciliated cells (left), Alveolar organoids retaining SPC$^+$ AT2 and HOPX$^+$ AT1 cells (middle), and Mixed organoids retaining both CC10$^+$ secretory and SPC$^+$ AT2 cells (right). CC10 (for secretory cells, red or green), Acetylated-Tubulin (Act-Tub, for ciliated cells, green), SPC (for AT2 cells, white), HOPX (for AT1 cells, white), and DAPI (blue). Scale bars, 50μm. **g,** Representative bright-field images of organoids under feeder-free condition with complete culture medium at passage 5. Insets show high-power view. Scale bars, 2,000μm. **h,** Representative IF images of mixed organoids cultured in complete medium at passage 5. CC10 (green), Act-Tub (red), SPC (white, left), p63 (for basal cells, white, right), and DAPI (blue). Insets (1, 2) show high-power view. Scale bars, 50μm. **i,** Quantification of each organoid types in complete medium at passage 0 and over passage 5; Airway organoids (CC10$^+$SPC$^-$; red), Alveolar organoids (CC10$^-$SPC$^+$; blue), and Mixed organoids (CC10$^+$SPC$^+$; grey). Data are presented as mean and s.e.m. (n=3 independent experiment). ***$p<0.001$.

1137

Figure 2. Enhanced differentiation of secretory cells into AT2 cells by inhibition of Notch activity upon lung injury.

a, A heatmap showing normalised expression data for secretory and AT2 cell markers that were differentially expressed in secretory cell-derived organoids (SCOs) or AT2 cell-derived organoids (ACOs) cultured with defined media at passage 10. Values are z-scores. **b,** Gene set

1143   enrichment analysis (GSEA) showing the gene activity of the three gene sets for secretory cells

1144   (top), AT2 cells (middle), and Notch signalling pathway-related in SCOs or ACOs **c,**

1145   Representative IF (top) and H&E (bottom) images of organoids in treatment with DMSO

1146   (control) and DAPT at day 14. DAPT (20μM) were treated every other day during organoid

1147   culture. CC10 (green), Acetylated-Tubulin (Act-Tub, red), and SPC (white), and DAPI (blue).

1148   Scale bar, 50μm. **d,** A heatmap showing normalised expression data for Notch signalling

1149   related, secretory and AT2 cell marker genes that were differentially expressed in SCOs with

1150   or without DAPT treatment for 14 days. Values are z-scores. **e,** GSEA with two gene sets

1151   representing markers for secretory (left) and AT2 cells (right) in SCOs with or without DAPT

1152   treatment. **f,** Experimental design of lineage-tracing analysis for contribution of secretory cells

1153   into   alveolar   lineages   by   inhibition   of   Notch   signalling   using   *Scgb1a1-*

1154   *CreER$^{TM/+}$;R26R$^{tdTomato/+}$* and *dnMAML$^{flox/+}$;Scgb1a1-CreER$^{TM/+}$;R26R$^{tdTomato/+}$* mice after

1155   bleomycin (Bleo) injury. Specific time points for tamoxifen injection and tissue analysis are

1156   indicated. **g, h,** Representative IF images showing the derivation of *Scgb1a1* lineage-labelled

1157   AT2 cells in PBS-treated control (**g**) or bleomycin-treated (**h**) mice at day 28. Tomato (for

1158   *Scgb1a1* lineage, red), SPC (white), and DAPI (blue). Scale bar, 100μm. **i,** Statistical

1159   quantification of *Scgb1a1$^+$* lineage-labelled AT2 cells at day 28 post PBS or bleomycin

1160   treatment. Each individual dot represents one section and data are presented as mean ± s.e.m.

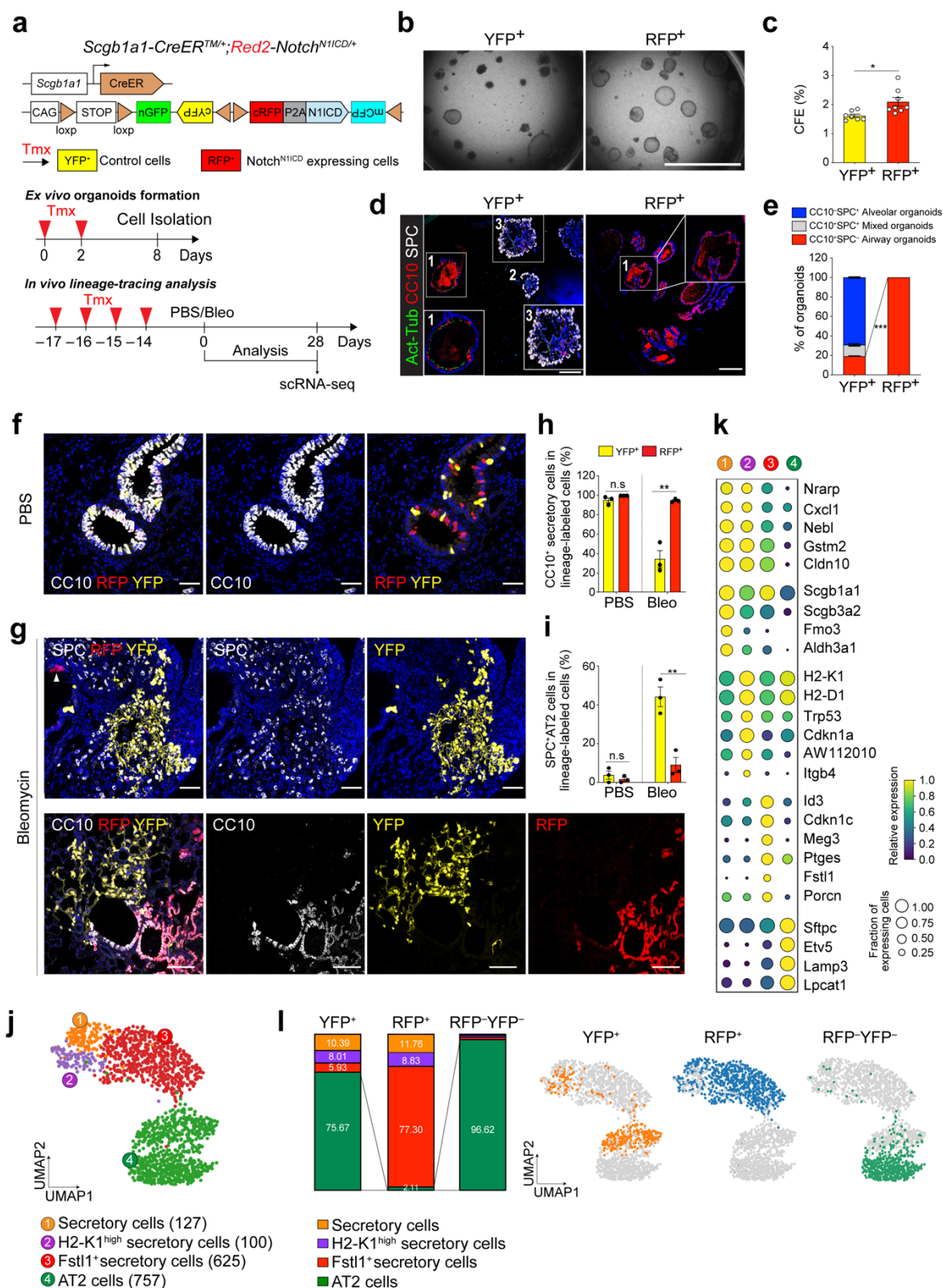1161   (n=2 biological replicates for PBS control, n=4 for bleomycin). ***p<0.001, n.s; not significant.

1162

1163

Figure 3. Impaired contribution of secretory cells into AT2 cell regeneration by sustained

Notch activity.

1166   **a,** Experimental design of *ex vivo* organoid co-culture with stromal cells, lineage-tracing

1167   analysis, and single-cell RNA-sequencing (scRNA-seq) analysis using *Scgb1a1-CreER$^{TM/+}$;*

1168   *Red2-Notch$^{N1ICD/+}$* mice after bleomycin injury. Specific time points for tamoxifen injection

1169   and analysis for tissue and scRNA-seq are indicated. **b,** Representative bright-field images of

1170   organoids derived from control YFP$^+$ (left) and *N1ICD*-expresing RFP$^+$ (right) cells. For

1171   organoids, 5,000 cells of YFP$^+$ or RFP$^+$ cells were co-cultured with stromal cells with 1:5 ratio

1172   for 14 days. Scale bar, 2,000μm. **c,** Statistical quantification of colony forming efficiency (CFE)

1173   of organoids in (**b**). Each individual dot represents one individual biological replicate and data

1174   are presented as mean and s.e.m. *$p<0.05$. **d,** Representative IF images of three distinctive

1175   types of organoids in (**b**); Airway organoids (denoted as 1), Alveolar organoids (denoted as 2),

1176   and Mixed organoids (denoted as 3). CC10 (for secretory cells, red), Act-Tub (for ciliated cells,

1177   green), SPC (for AT2 cells, white), and DAPI (blue). Insets (1 and 3) show high-power view.

1178   Scale bars, 50μm. **e,** Quantification of each organoid types in (**d**); Airway organoids

1179   (CC10$^+$SPC$^-$; red), Alveolar organoids (CC10$^-$SPC$^+$; blue), and Mixed organoids (CC10$^+$SPC$^+$;

1180   grey). Data are presented as mean and s.e.m (n=3 biological replicates). ***$p<0.001$. **f,**

1181   Representative IF images showing the derivation of YFP$^+$ or RFP$^+$ cells in control mice at day

1182   28 post PBS treatment. YFP (yellow), RFP (red), CC10 (white), and DAPI (blue). Scale bar,

1183   50μm. **g,** Representative IF images showing the derivation of YFP$^+$ or RFP$^+$ cells at day 28

1184   post bleomycin treatment. YFP (yellow), RFP (red), SPC (top, white), CC10 (bottom, white),

1185   and DAPI (blue). Arrowhead points to RFP$^+$ cells. Scale bar, 50μm. **h, i,** Statistical

1186   quantification of CC10$^+$ secretory (**h**) and SPC$^+$ AT2 (**i**) cells derived from YFP$^+$ or RFP$^+$ cells

1187   at day 28 post PBS or bleomycin treatment. **$p<0.01$. **j,** Secretory and AT2 cell population

1188   were further analysed from scRNA-seq results (Extended Data Fig. 7b). Clusters of YFP$^+$ and

1189   RFP$^+$ lineage-labelled or YFP$^-$RFP$^-$ non-lineage labelled epithelial cells (1,609) from 10x

1190   Genomics 3' single-cell RNA sequencing (scRNA-seq) analysis visualised by UMAP,

1191   assigned by specific colours. Number of cells in the individual cluster is depicted in the figure.

1192   **k,** Gene expression of key markers in each distinctive cluster. The size of the circle represents

1193   the fraction of cells expressing the gene and the colour represents the relative expression of

1194   each gene. **l,** Quantification (left) and UMAP (right) of distribution of each cluster across

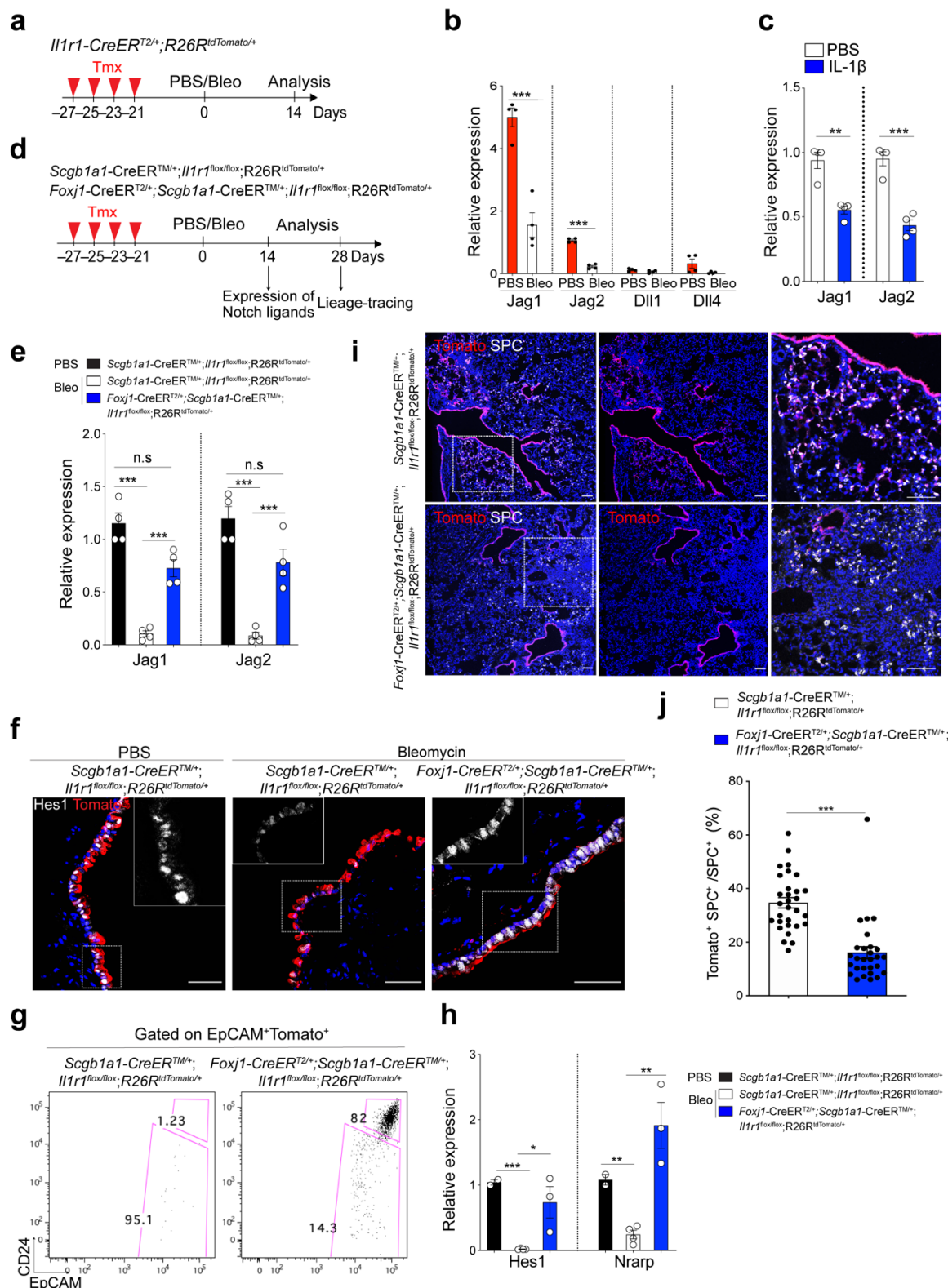1195   indicated lineage-labelled cells after injury.

1196

1197

Figure 4. Regulation of Notch ligand expression in ciliated cells by IL-1β signalling.

a, Experimental design for isolation of *Il1r1*-expressing ciliated cells after PBS or bleomycin treatment using *Il1r1-CreER$^{T2/+}$;R26R$^{tdTomato/+}$* mice. Specific time points for tamoxifen injection are indicated and tissue was analysed at day 14 post PBS or bleomycin treatment. **b,**

1202   Quantitative PCR (qPCR) analysis showing the expression of Notch ligands in isolated lineage-

1203   labelled ciliated cells (EpCAM$^+$*Il1r1*$^+$CD24^{high}). ***p<0.001. **c,** qPCR analysis showing the

1204   expression of *Jag1* and *Jag2* in cultured ciliated cells treated with PBS or IL-1β. Isolated

1205   ciliated cells (EpCAM$^+$*Il1r1*$^+$CD24^{high}) from *Il1r1-CreER$^{T2/+}$;R26R$^{tdTomato/+}$* mouse lungs after

1206   two doses of tamoxifen were cultured in Matrigel for 24 hrs in the presence of PBS or IL-1β

1207   (10ng/ml) *in vitro*. **p<0.01, ***p<0.001. **d,** Experimental design for lineage-tracing analysis

1208   of secretory cells after PBS or bleomycin treatment using *Scgb1a1-*

1209   *CreER$^{TM/+}$;Il1r1$^{flox/flox}$;R26R$^{tdTomato/+}$* or *Foxj1-CreER^{T2};Scgb1a1-CreER$^{TM/+}$;Il1r1$^{flox/flox}$;*

1210   *R26R$^{tdTomato/+}$* mice. Specific time points for tamoxifen injection and tissue analysis are

1211   indicated. **e,** qPCR analysis showing the expression of *Jag1* and *Jag2* in isolated ciliated cells

1212   (Tom$^+$EpCAM$^+$CD24^{high}) after treatment of PBS or bleomycin. ***p<0.001, n.s; not

1213   significant. **f,** Representative IF images showing Hes1 expression in lineage-labelled secretory

1214   cells after bleomycin at day 14 post injury in the indicated genotype: Tomato (for *Scgb1a1*

1215   lineage, red), Hes1 (white), and DAPI (blue). Insets show high-power view of Hes1 expression.

1216   Scale bars, 50μm. **g,** Flow cytometry sorting strategy for lineage-labelled secretory cells after

1217   PBS or bleomycin injury. EpCAM$^+$CD24$^-$ cells gated from EpCAM$^+$Tomato$^+$ were used for

1218   isolation of lineage-labelled secretory cells and qPCR analysis. **h,** qPCR analysis of

1219   downstream target genes of Notch signalling including *Hes1* and *Nrarp* from isolated lineage-

1220   labelled secretory cells in (**g**). *p<0.05, **p<0.01, **p<0.001. **i,** Representative IF images

1221   showing the derivation of *Scgb1a1*$^+$ lineage-labelled AT2 cells in PBS-treated control or

1222   bleomycin-treated mice at day 28. Tomato (for *Scgb1a1* lineage, red), SPC (white), and DAPI

1223   (blue). White boxed insets show high-power view (right panel). Scale bar, 100μm. **j,** Statistical

1224   quantification of Tomato$^+$SPC$^+$ AT2 cells at day 28 post bleomycin treatment in (**f**). Each

1225   individual dot represents one section from four (*Scgb1a1-CreER$^{TM/+}$;Il1r1$^{flox/flox}$;R26R$^{tdTomato/+}$*)

1226   or three (*Foxj1-CreER^{T2};Scgb1a1-CreER$^{TM/+}$;Il1r1$^{flox/flox}$;R26R$^{tdTomato/+}$*) biological replicates.

1227   Data are presented as mean ± s.e.m. ***p<0.001.

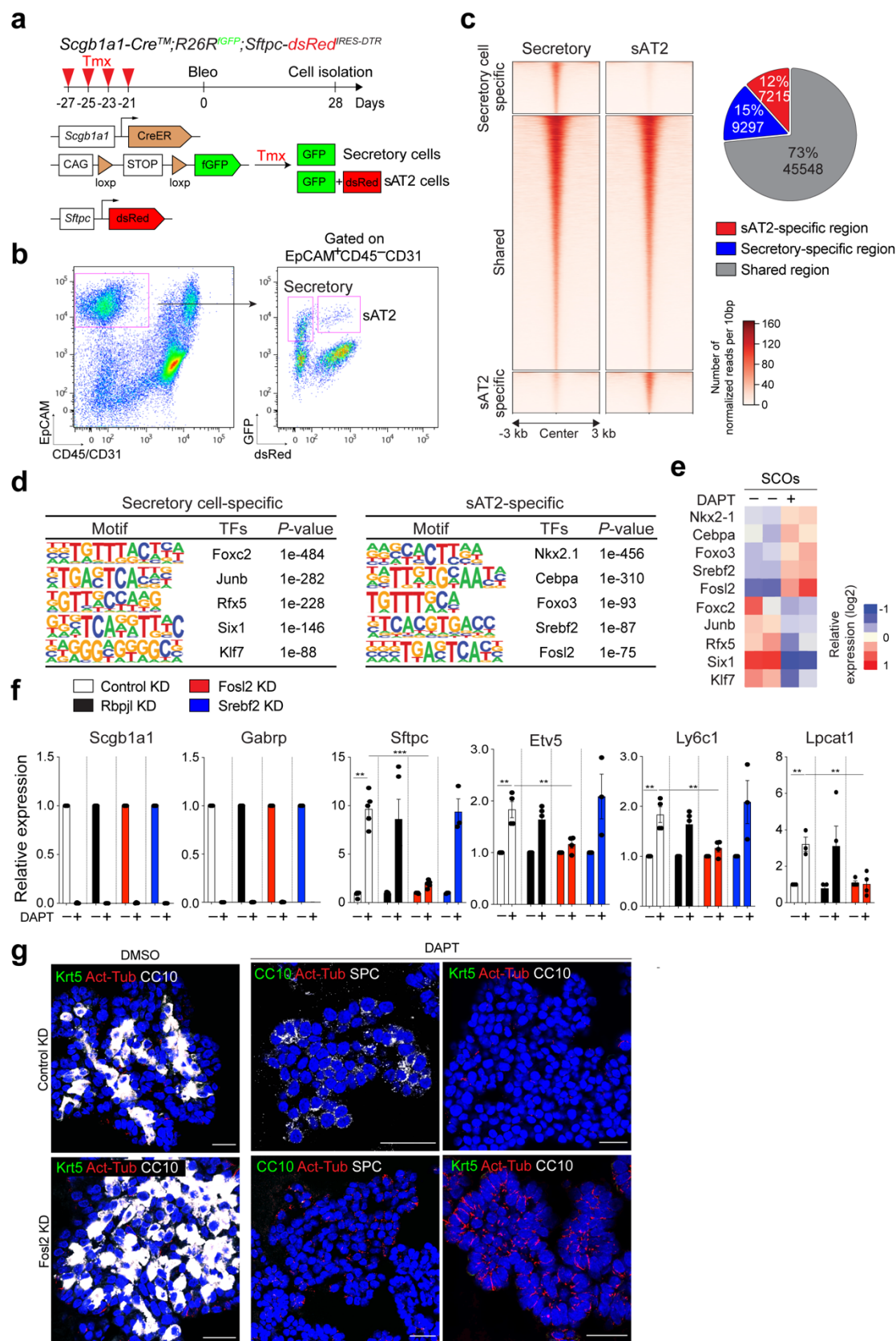1228

1229

Figure 5. **Fosl2/Fra2-mediated AP-1 activity is required for the fate conversion of secretory cells into AT2 cells**.

44

1232   **a,** Experimental design for isolation of secretory (GFP$^+$dsRed$^-$) and secretory-derived AT2

1233   (sAT2, GFP$^+$dsRed$^+$) cells using *Scgb1a1-CreER$^{TM/+}$;R26R$^{fGFP/+}$;Sftpc-dsRed$^{IRES-DTR/+}$* mouse

1234   post bleomycin injury. Specific time points for tamoxifen injection and isolation of cells are

1235   indicated. **b,** Representative flow cytometry analysis for isolation of secretory (GFP$^+$dsRed$^-$)

1236   and sAT2 (GFP$^+$dsRed$^+$) cells. **c,** A heatmap showing ATAC-seq peaks representing open

1237   chromatin regions in secretory cells (left) and sAT2 cells (right). Secretory-specific, shared,

1238   and sAT2-specific peaks are shown. Regions of a pie chart presenting the proportion of

1239   secretory-specific (blue), sAT2-specific (red), and shared regions (grey). **d,** Top five motif

1240   matrices and transcription factors predicted by the HOMER *de novo* motif analysis using

1241   secretory-specific and sAT2-specific open regions. **e,** A heatmap showing the expression levels

1242   of transcription factors predicted by the motif analysis (Fig. 5d) in secretory cell-derived

1243   organoids (SCOs) with or without DAPT treatment (20μM). **f,** qPCR analysis of the markers

1244   for secretory (*Scgb1a1* and *Gabrp*) and AT2 cells (*Sftpc*, *Etv5*, *Ly6c1*, and *Lpcat1*) in SCOs

1245   with or without DAPT treatment after knockdown of control (white), Rbpjl (black), Fosl2 (red),

1246   and Srebf2 (blue). **p<0.01, ***p<0.001. **g,** Representative IF images of secretory cell-

1247   derived control KD or *Fosl2* KD organoids treated with DMSO or DAPT (20μM). Single cells

1248   dissociated from SCOs at passage 10-12 were cultured in feeder-free condition for 7 days and

1249   further maintained with DMSO or DAPT for another 7 days. CC10 (white, left and right panels;

1250   green, middle panel), SPC (white, middle panels), Krt5 (green, left and right panels), Act-Tub

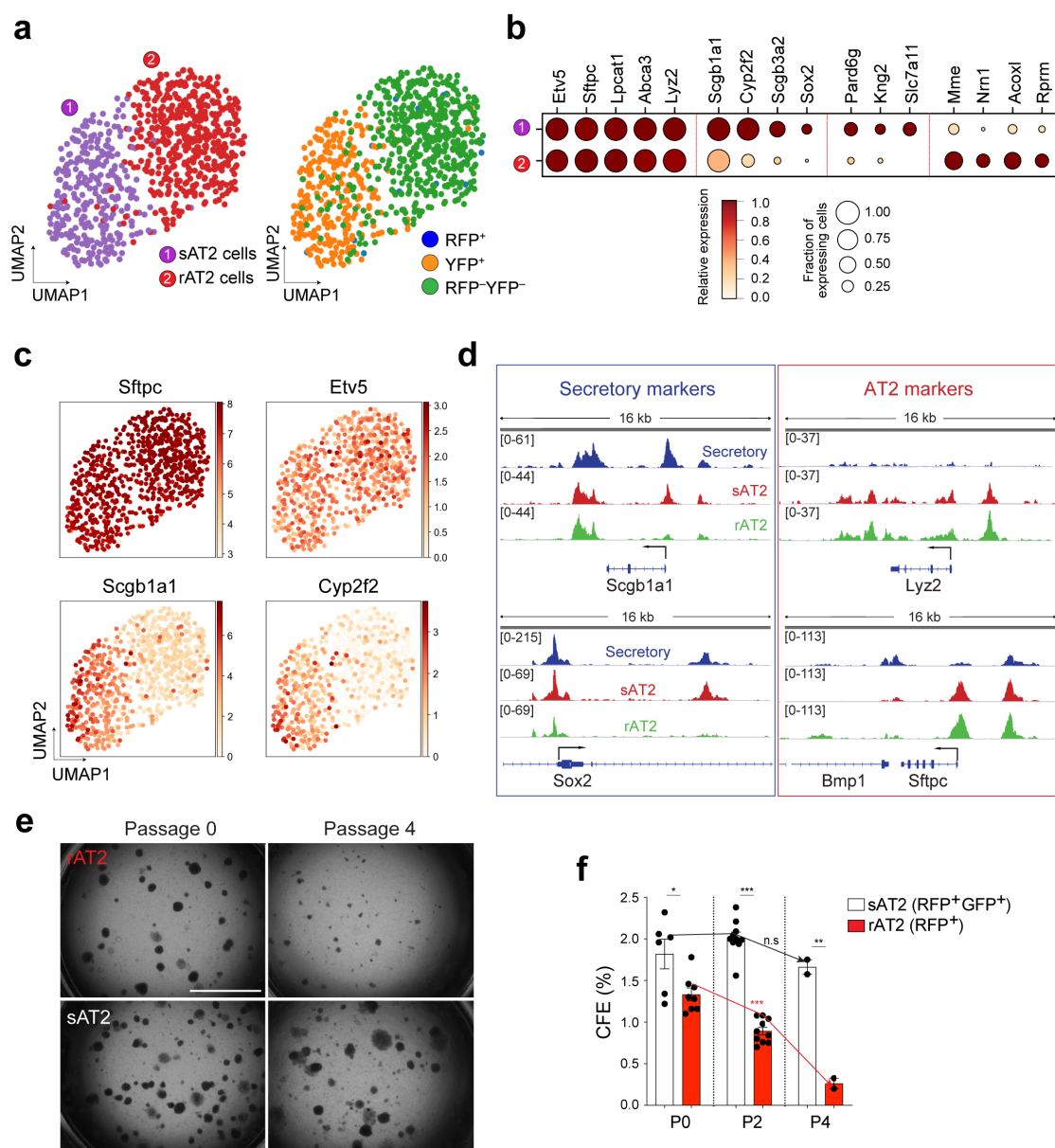1251   (red), and DAPI (blue). Scale bars, 50μm.

1252

1253

1254

Figure 6. Distinctive features of secretory-derived AT2 cells.

a, UMAP visualisation of two distinctive AT2 cell clusters sAT2 (secretory cell-derived AT2, YFP⁺SPC⁺ cluster); rAT2 (resident AT2, YFP⁻RFP⁻ non-lineage labelled SPC⁺ cluster) from scRNA-seq analysis of $Scgb1a1$-$CreER^{TM/+}$;$Red2$-$Notch^{N1ICD/+}$ mice in **Fig. 3j**. **b,** Gene expression of key markers in sAT2 and rAT2 cell clusters. **c,** UMAP visualisation of the log-transformed ($\log_{10}$(TPM+1)), normalised expression of selected marker genes ($Sftpc$ and $Etv5$ for AT2 cells. $Scgb1a1$ and $Cyp2f2$ for secretory cells) in distinctive clusters shown in (**a**). **d,** Signal track images showing open regions of markers for secretory (Scgb1a1 and Sox2) and AT2 cells (Lyz2 and Sftpc) mapped in secretory (blue), sAT2 (red), and rAT2 cells (green)

46

1264   from the result of **Fig. 5c**. **e,** Representative bright-field images of organoids derived from

1265   rAT2 (top) or sAT2 (bottom) cells: Experiment scheme for labelling with tamoxifen is same

1266   as **Fig. 5a**. *Scgb1a1-CreER$^{TM/+}$;R26R$^{fGFP/+}$;Sftpc-dsRed$^{IRES-DTR/+}$* mice was given four doses of

1267   tamoxifen followed by bleomycin injury. Isolated GFP$^+$dsRed$^+$(sAT2) and GFP$^-$dsRed$^+$(rAT2)

1268   cells at 2 months post bleomycin injury were co-cultured with stromal cells with 1:5 ratio.

1269   Images show the organoids at passage 0 and 4. Scale bar, 2,000μm. **f,** Statistical quantification

1270   of colony forming efficiency (CFE) of indicated organoids. Each individual dot represents

1271   individual biological replicate and data are presented as mean and s.e.m. *$p<0.05$, **$p<0.01$,

1272   ***$p<0.001$.

1273

1274
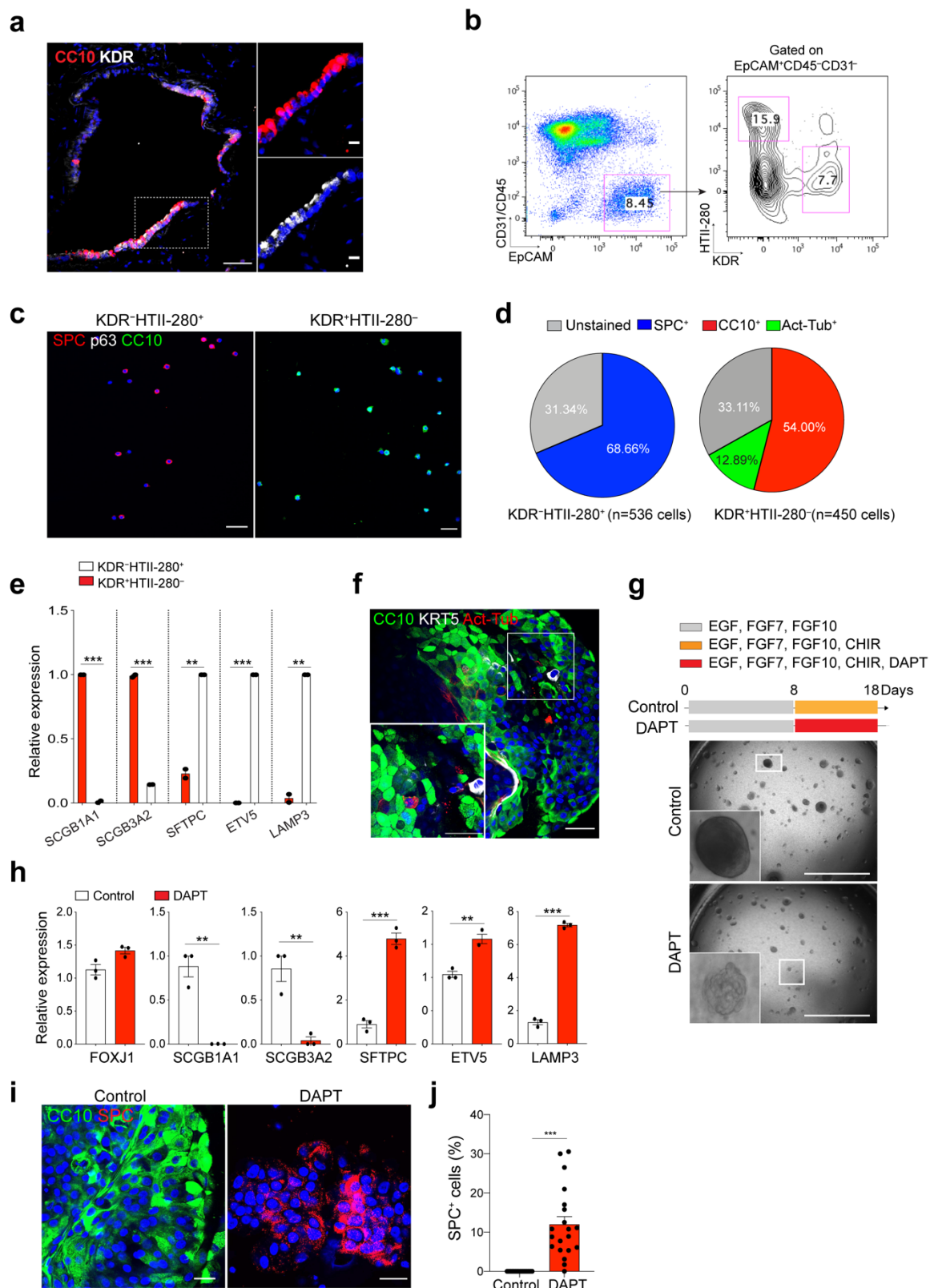
1275 **Figure 7**. **Differentiation plasticity of secretory cells into AT2 cells by inhibition of Notch**

1276 **signalling in human lungs**.

1277   **a,** IF images showing the expression of KDR in secretory cells in the lung from normal donors.

1278   CC10 (red), KDR (white), and DAPI (blue). White boxed insets show high-power view. Scale

1279   bar, 50μm and 10μm (inset). **b,** Representative flow cytometry analysis for isolation of

1280   KDR$^+$HTII-280$^-$ or KDR$^-$HTII-280$^+$ cells from human lung parenchymal tissues. **c,**

1281   Representative IF images of cytospin staining from freshly sorted KDR$^-$HTII-280$^+$ or

1282   KDR$^+$HTII-280$^-$ population. SPC (for AT2 cells, red), p63 (for basal cells, white), CC10 (for

1283   secretory cells, green) and DAPI (blue). Scale bars, 100μm. **d,** Quantification of SPC$^+$, CC10$^+$,

1284   and Act-Tub$^+$ cells revealed in cytospin staining from KDR$^-$HTII-280$^+$ or KDR$^+$HTII-280$^-$

1285   cells in **Fig. 7c**. **e,** qPCR analysis of the markers for secretory (*SCGB1A1* and *SCGB3A2*) and

1286   AT2 (*SFTPC*, *ETV5*, and *LAMP3*) cells in freshly isolated KDR$^+$HTII-280$^-$ (red bars) or

1287   KDR$^-$HTII-280$^+$ (white bars) cells. **p<0.01, ***p<0.001. **f,** Representative IF images of

1288   KDR$^+$ cell-derived organoids at first passage. KDR$^+$HTII-280$^-$ cells were cultured in the basic

1289   medium supplemented with EGF, NOG, FGF7, and FGF10 for 3 weeks. CC10 (green), Act-

1290   Tub (red), KRT5 (white), and DAPI (blue). Scale bar, 50μm. **g,** Representative bright-field

1291   images of organoids derived from KDR$^+$HTII-280$^-$ cells with or without DAPT treatment

1292   (20μM) at passage 1. Isolated KDR$^+$HTII-280$^-$ cells were cultured with airway cell culture

1293   medium (See **Methods**) supplemented with EGF (50ng/ml), FGF7 (100ng/ml), and FGF10

1294   (100ng/ml) for 8 days, followed by inclusion of CHIR99021 (2μM) for additional 10 days with

1295   or without DAPT (20μM). Scale bar, 2,000μm. **h**, qPCR analysis of the markers for secretory

1296   cells (*SCGB1A1* and *SCGB3A2*) and AT2 cells (*SFTPC*, *ETV5*, and *LAMP3*) in organoids

1297   derived KDR$^+$HTII-280$^-$ cells without (white bars) or with DAPT treatment (red bars). Each

1298   individual dot represents individual biological replicate and data are presented as mean ± s.e.m.

1299   **p<0.01, ***p<0.001. **i**, Representative IF images of KDR$^+$ cell-derived organoids treated

1300   with DMSO or DAPT (20μM). CC10 (green), SPC (red), and DAPI (blue). Scale bar, 50μm. **j**,

1301   Quantification of the frequency of SPC$^+$ cells in the control or DAPT treated organoids. Each

1302   individual dot represents one organoid and data are presented as mean ± s.e.m (n=3

1303   independent biological replicates). ***p<0.001.

1304 **Extended Data**

1305
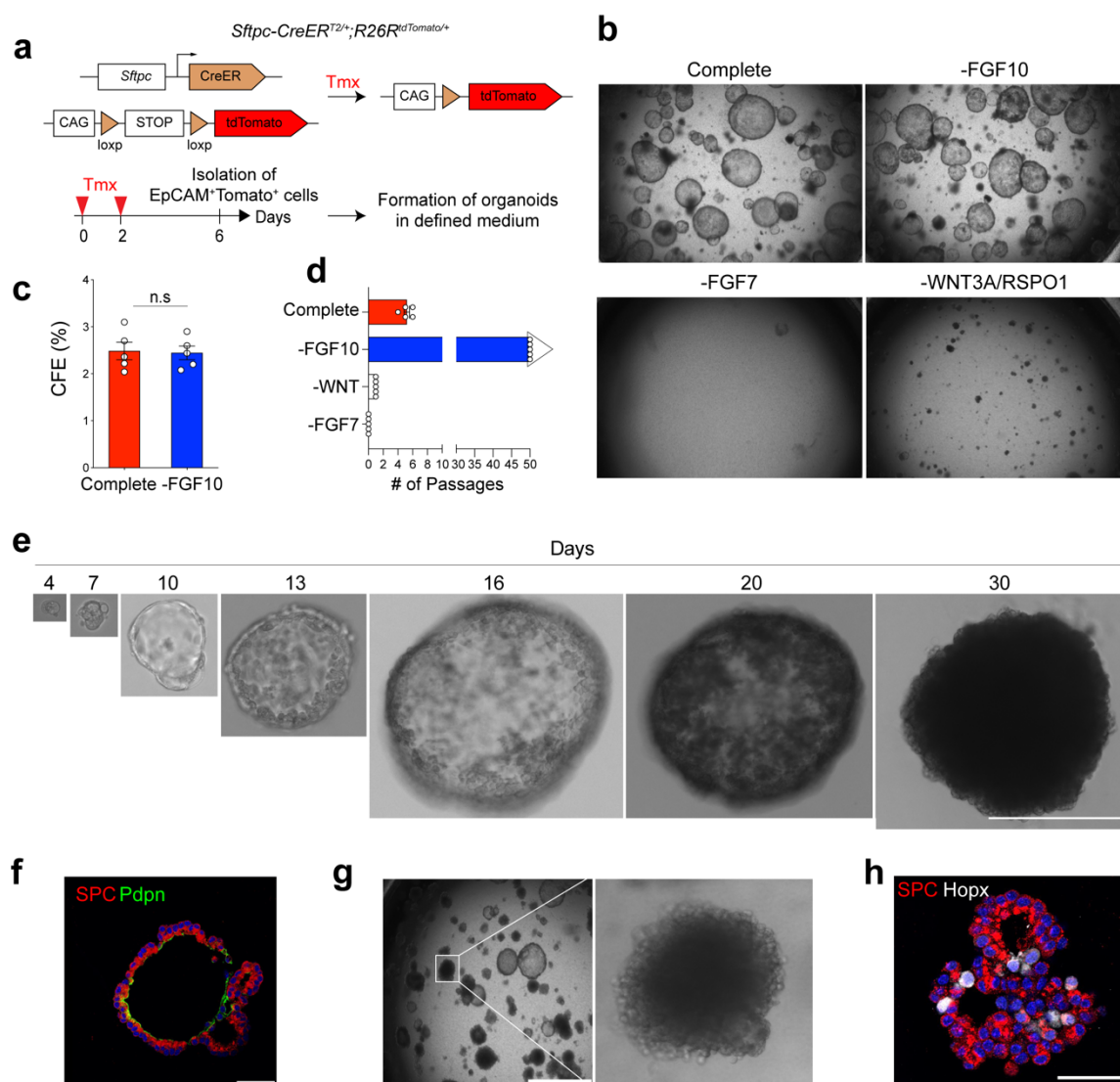
1306 **Extended Data Figure 1. Establishment of feeder-free organoids derived from AT2 cells.**

1307 **a,** Schematics of experimental design for isolation of *Sftpc* lineage-labelled AT2 cells at

1308 indicated time points after tamoxifen treatment. **b,** Representative bright-field images of

1309 organoids derived from lineage-labelled *Tomato*$^+$*Sftpc*$^+$ cells in indicated conditions; complete

1310 medium with WNT3A, RSPO1 (R-spondin 1), EGF, FGF7, FGF10, and NOG (Noggin),

1311 withdrawal of indicated factors (−FGF10, −FGF7, or −WNT3A/RSPO1). Scale bar, 2,000μm.

1312 **c, d,** Statistical quantification of colony forming efficiency (**c**) and passaging numbers (**d**) of

1313 organoids. Each individual dot represents individual biological replicate and data are presented

1314 as mean and s.e.m. n.s; not significant. **e,** Representative serial bright-field images of a lung

1315 organoid growing originated from single *Tomato*$^+$*Sftpc*$^+$ cells at the indicated time points.

1316 Magnifications: X20 (day 4 and 7), X10 (day10 and 13), and X4 (day 16, 20, and 30). Scale
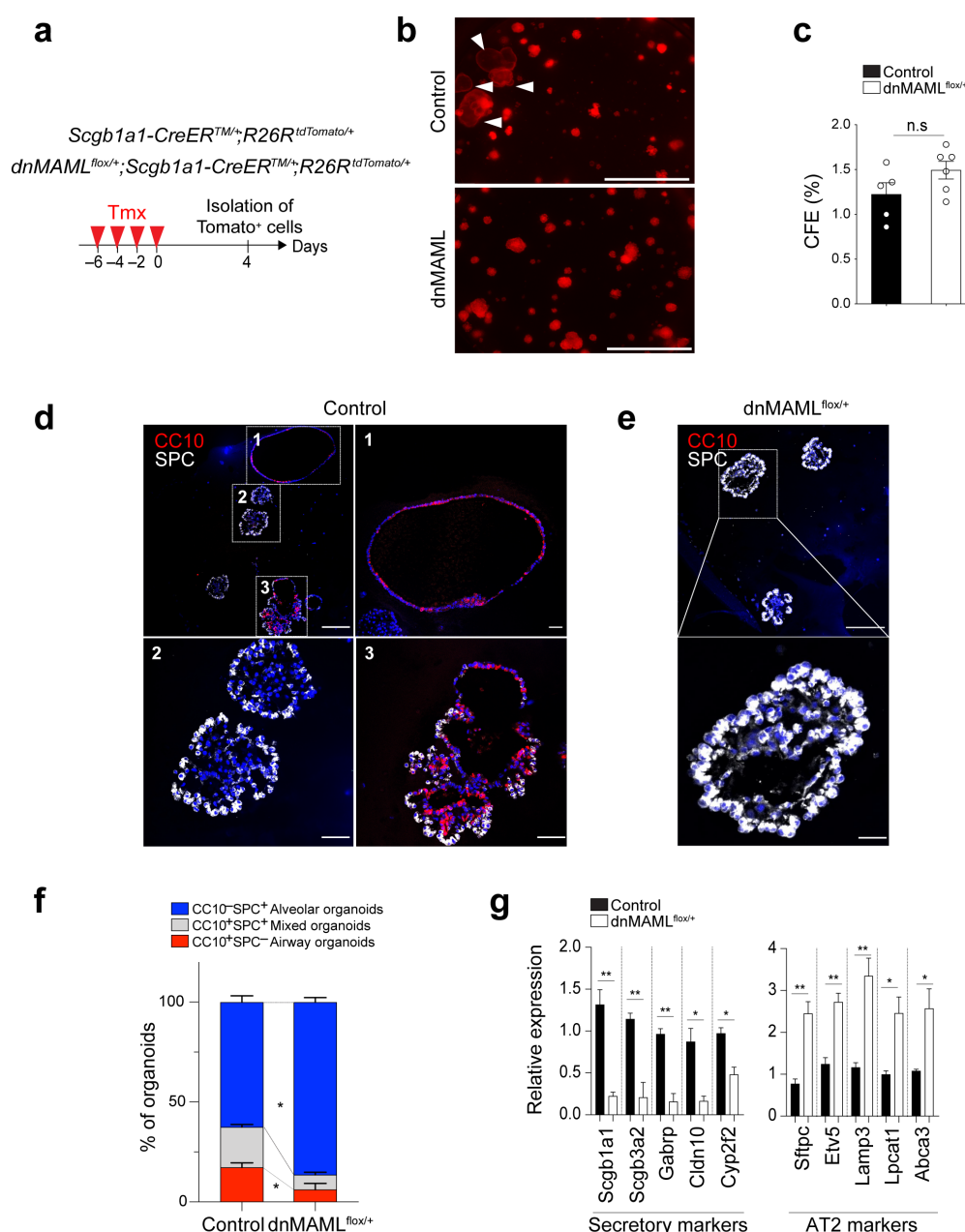
50

1317   bars, 400μm. **f,** A representative immunofluorescence (IF) image of organoids derived from

1318   *Tomato$^+$Sftpc$^+$* cells at the first passage under feeder-free condition with complete culture

1319   medium. SPC (for AT2 cells, red), Pdpn (for AT1 cells, green), and DAPI (blue). Scale bars,

1320   50μm. **g,** Representative bright-field images of organoids under feeder-free condition with

1321   complete culture medium at passage 5. Insets (left) show high-power view (right). Scale bars,

1322   2,000μm. **h,** Representative IF images of mixed organoids cultured in complete medium at

1323   passage >5. SPC (red), Hopx (white), and DAPI (blue). Scale bars, 50μm.

1324

1325
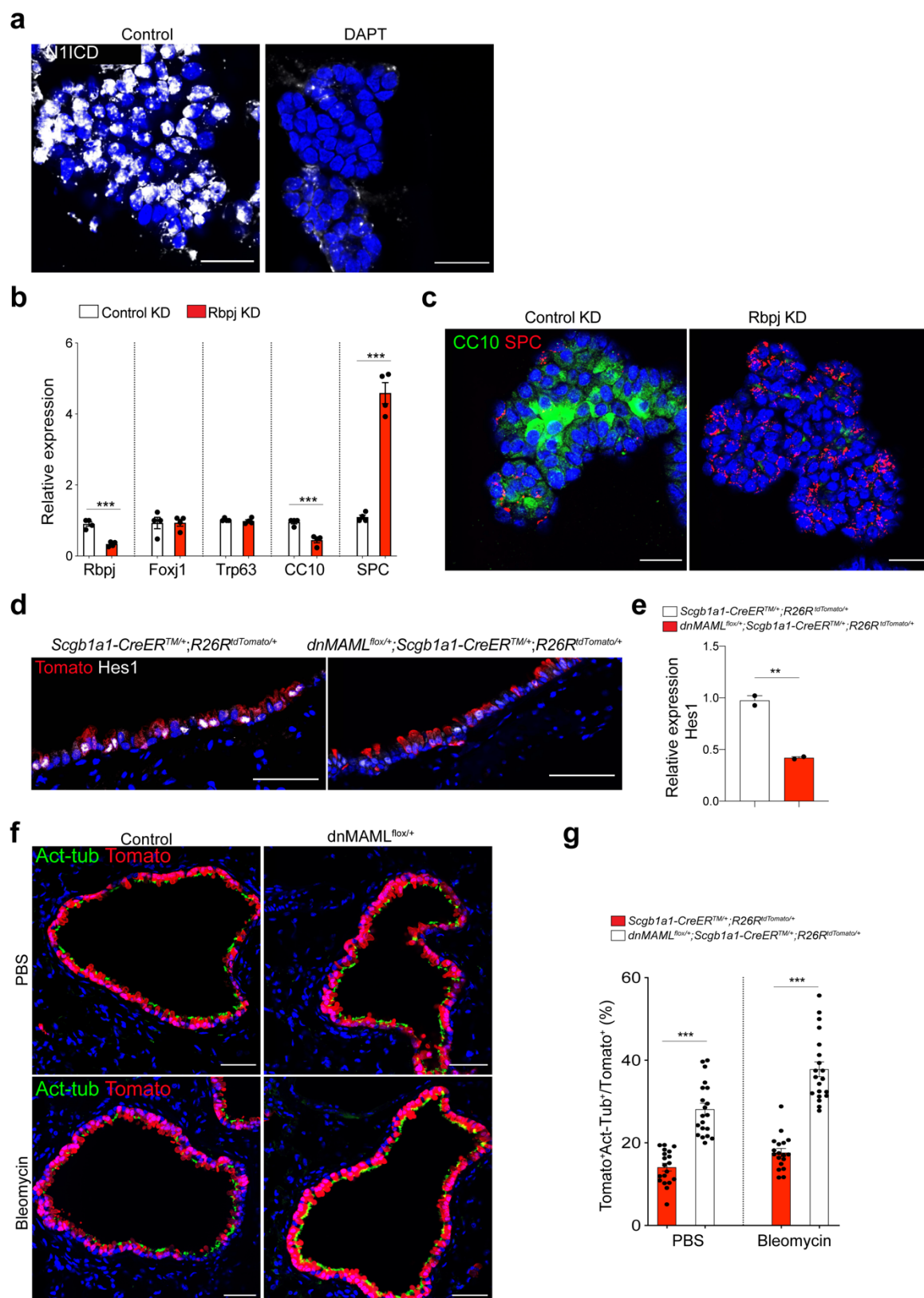
1326 **Extended Data Figure 2. Interference of Notch activity in secretory cell-derived**

1327 **organoids (SCOs) enhances the differentiation into AT2 lineages.**

1328   **a**, Representative IF images showing nuclear localisation of intracellular domain of Notch 1

1329   (N1ICD) in SCOs at passage 5 with or without DAPT (20μM). CC10 (red), N1ICD (white),

1330   and DAPI (blue). Scale bars, 50μm. **b,** qPCR analysis of gene expression in control (control

1331   KD) or *Rbpj* knock-downed (*Rbpj* KD) organoids. Each individual dot represents one

1332   individual experiment (n=4 biological replicates) and data are presented as mean ± s.e.m.

1333   ***p<0.001. **c,** Representative IF images of control KD or *Rbpj* KD organoids: CC10 (green),

1334   SPC (red), and DAPI (blue). Scale bars, 50μm. **d,** Representative IF images showing Hes1

1335   expression in lineage-labelled secretory cells after tamoxifen treatment in the indicated

1336   genotype: Tomato (for *Scgb1a1* lineage, red), Hes1 (white), and DAPI (blue). Scale bars, 50μm.

1337   **e,** qPCR analysis of *Hes1* expression in isolated EpCAM$^+$Tomato$^+$. Data are presented as mean

1338   ± s.e.m (n=2 individual biological replicate). **p<0.01. **f,** Representative IF images showing

1339   the derivation of lineage-labelled Act-Tub$^+$ ciliated cells in PBS- or bleomycin-treated lungs

1340   of *Scgb1a1-CreER$^{TM/+}$;R26R$^{tdTomato/+}$* or *dnMAML$^{flox/+}$;Scgb1a1-CreER$^{TM/+}$;R26R$^{tdTomato/+}$*

1341   mice. Tomato (for *Scgb1a1* lineage, red), Acetylated-Tubulin (Act-Tub, green), and DAPI

1342   (blue). Scale bar, 50μm. **g,** Statistical quantification of lineage-labelled ciliated cells at day 28

1343   post PBS or bleomycin treatment. Each individual dot represents one section and data are

1344   presented as mean ± s.e.m. (n=2 biological replicates for PBS control and bleomycin).

1345   ***p<0.001.

1346

a, Experimental design for isolation of lineage-labelled secretory cells from *Scgb1a1-CreER$^{TM/+}$;R26R$^{tdTomato/+}$* and *dnMAML$^{flox/+}$;Scgb1a1-CreER$^{TM/+}$;R26R$^{tdTomato/+}$* mice at indicated time points after tamoxifen treatment. **b,** Representative fluorescent images of organoids derived from control or *dnMAML*-expressing lineage-labelled secretory cells. 5,000 cells of lineage-labelled secretory cells (Tomato$^+$EpCAM$^+$CD45$^-$CD31$^-$) isolated from *Scgb1a1-CreER$^{TM/+}$;R26R$^{tdTomato/+}$* or *dnMAML$^{flox/+}$;Scgb1a1-CreER$^{TM/+}$;R26R$^{tdTomato/+}$* mouse

Extended Data Figure 3. Organoid co-culture shows enhanced differentiation of secretory cells into AT2 cells by downregulation of Notch activity.

1347

1348

1349

1350

1351

1352

1353

1354

1355

1356   lungs were co-cultured with stromal cells with 1:5 ratio for 14 days. Arrowheads point to cystic

1357   airway-like organoids. Scale bar, 2,000μm. **c,** Statistical quantification of colony forming

1358   efficiency of organoids. Each individual dot represents one biological replicate and data are

1359   presented as mean and s.e.m. n.s; not significant. CFE; Colony forming efficiency units. **d,**

1360   Representative IF images of three distinctive types of organoids derived from control secretory

1361   cells; Airway organoids (CC10$^+$SPC$^-$; denoted as 1), Alveolar organoids (CC10$^-$SPC$^+$; denoted

1362   as 2), and Mixed organoids (CC10$^+$SPC$^+$; denoted as 3). CC10 (for secretory cells, red), SPC

1363   (for AT2 cells, white), and DAPI (blue). Insets (1, 2 and 3) show high-power view. Scale bars,

1364   50μm and 10μm (in high-power view). **e,** Representative IF images of alveolar organoids

1365   derived from *dnMAML*-expressing secretory cells. CC10 (for secretory cells, red), SPC (for

1366   AT2 cells, white), and DAPI (blue). Insets show high-power view. Scale bars, 50μm (10μm in

1367   high-power view). **f,** Quantification of each organoid types derived from *Scgb1a1-*

1368   *CreER$^{TM/+}$;R26R$^{tdTomato/+}$* or *dnMAML$^{flox/+}$;Scgb1a1-CreER$^{TM/+}$;R26R$^{tdTomato/+}$* mice in (**d** and

1369   **e**); Airway organoids (CC10$^+$SPC$^-$; red), Alveolar organoids (CC10$^-$SPC$^+$; blue), and Mixed

1370   organoids (CC10$^+$SPC$^+$; grey). Data are presented as mean and s.e.m (n=3 biological replicates).

1371   *p<0.001. **g,** qPCR analysis of markers for secretory (*Scgb1a1, Scgb3a2, Gabrp, Cldn10,* and

1372   *Cyp2f2*) and AT2 (*Sftpc, Etv5, Lamp3, Lpcat1,* and *Abca3*) cells in organoids isolated from

1373   *Scgb1a1-CreER$^{TM/+}$;R26R$^{tdTomato/+}$* (black bars) and dnMAML$^{flox/+}$;*Scgb1a1-CreER$^{TM/+}$;*

1374   *R26R$^{tdTomato/+}$* mice (white bars). *p<0.05, **p<0.01.

1375
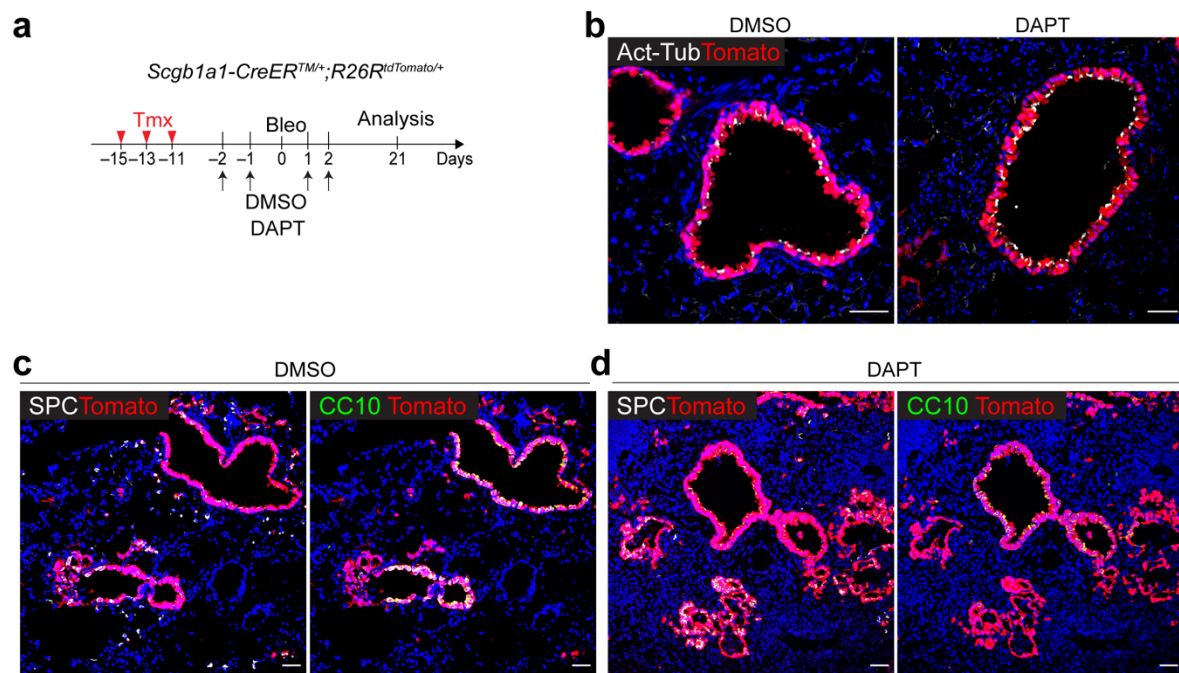
Extended Data Figure 4. Pharmacological inhibition of Notch activity by DAPT treatment enhances the differentiation of secretory cells into AT2 cells during injury repair.

a, Experimental design of lineage-tracing analysis of *Scgb1a1-CreER$^{TM/+}$;R26R$^{tdTomato/+}$* mice after bleomycin injury. DMSO or DAPT (50mg/kg body weight) was administrated *via* intraperitoneally as indicated time points. **b**, Representative IF images showing the increased *Scgb1a1$^+$* lineage-labelled Act-Tub$^+$ ciliated cells in DAPT-treated mouse lungs at day 21 post bleomycin injury compared to DMSO control mice. Tomato (for *Scgb1a1* lineage, red), Acetylated Tubulin (Act-Tub, white), and DAPI (blue). Scale bar, 50μm. **c,d**, Representative IF images showing the derivation of *Scgb1a1$^+$* lineage-labelled SPC$^+$ AT2 (left) or CC10$^+$ secretory cells (right) in DMSO control (**c**) or DAPT-treated (**d**) mice at day 21 post bleomycin injury. Tomato (for *Scgb1a1* lineage, red), SPC (white), CC10 (green), and DAPI (blue). Scale bar, 100μm.

56

1390

57
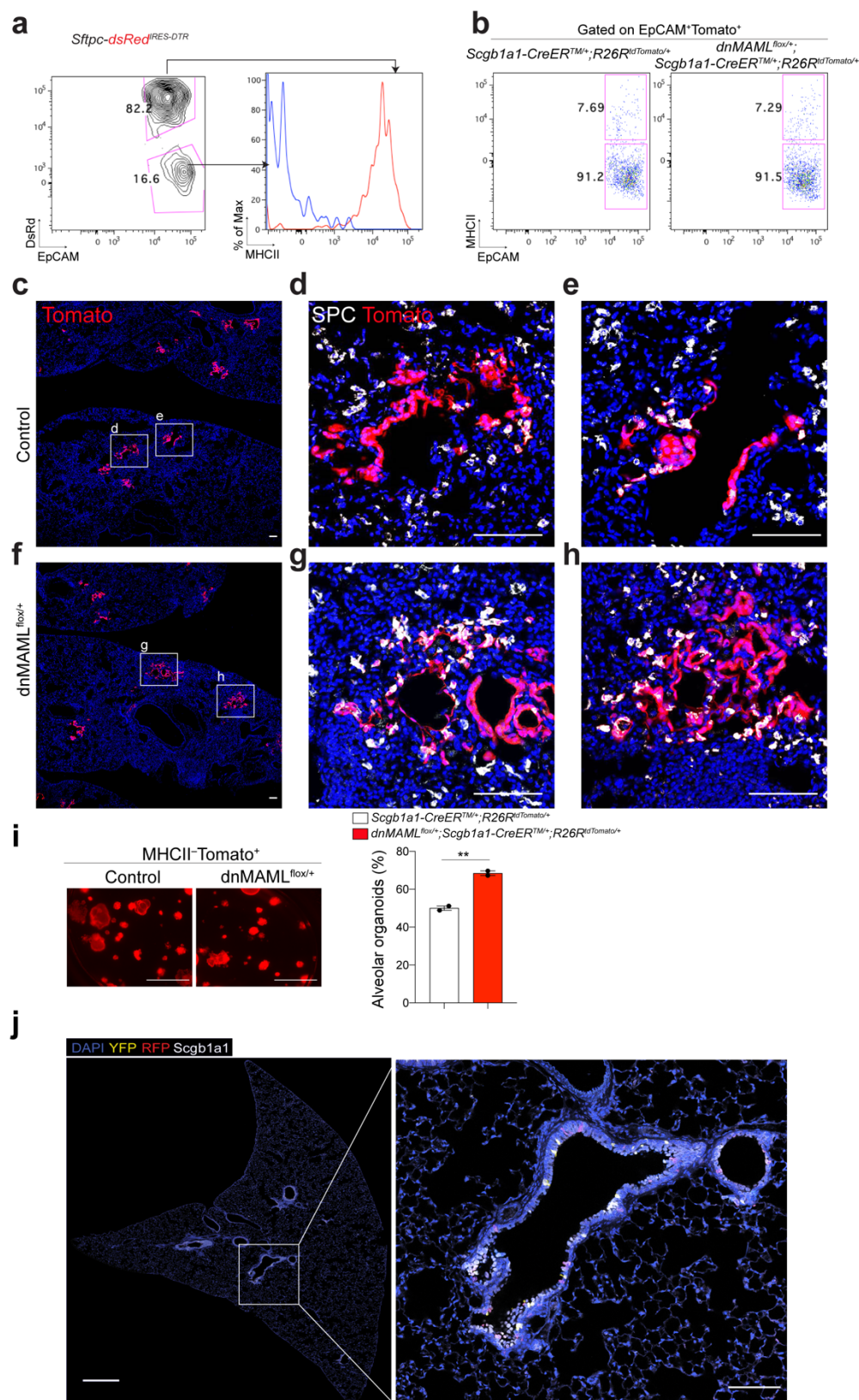
1391 **Extended Data Figure 5. Transplantation of secretory cells, after excluding lineage-**

1392 **labelled AT2 cells, reveals enhanced the differentiation of secretory cells into AT2**

1393 **cells via Notch inhibition.**

1394 **a,** MHCII expression marks AT2 cells. Representative flow cytometry analysis of MHCII

1395 expression in SPC$^+$ AT2 (EpCAM$^+$dsRed$^+$) or non-AT2 (EpCAM$^+$dsRed$^-$) cells from *Sftpc-*

1396 *dsRed$^{IRES-DTR}$* reporter mice. Sftpc-IRES-DTR-P2A-dsRed (*Sftpc-dsRed$^{IRES-DTR}$*) reporter

1397 mouse was used to monitor SPC-expressing AT2 cells based on the expression of dsRed (See

1398 **Methods**). Numbers adjacent to the outlined area indicate the percentage of populations. **b,**

1399 Flow cytometry analysis to exclude lineage-labelled AT2 cells, including CC10$^+$SPC$^+$ dual-

1400 positive cells, from *dnMAML$^{flox/+}$;Scgb1a1-CreER$^{TM/+}$;R26R^{tdTomato} $^{/+}$* or *Scgb1a1-*

1401 *CreER$^{TM/+}$;R26R$^{tdTomato/+}$* mouse lungs. **c-h,** Representative IF image of engrafted lineage-

1402 labelled secretory cells (EpCAM$^+$Tomato$^+$MHCII$^-$) isolated from *Scgb1a1-*

1403 *CreER$^{TM/+}$;R26R$^{tdTomato/+}$* (**c-e**) or *dnMAML$^{flox/+}$;Scgb1a1-CreER$^{TM/+}$;R26R$^{tdTomato/+}$* (**f-h**) mouse

1404 lungs at day 14 post transplantation. 20,000 cells of EpCAM+Tomato+MHCII$^-$ were engrafted

1405 into injured lung at day 7 after bleomycin injury. Tomato (for *Scgb1a1* lineage, red), SPC

1406 (white), and DAPI (blue). Scale bars, 100μm. **i,** Representative fluorescent images of organoids

1407 (top) and statistical quantification of colony forming efficiency of alveolar organoids (left)

1408 derived from lineage-labelled AT2 cells isolated from control (*Scgb1a1-*

1409 *CreER$^{TM/+}$;R26R$^{tdTomato/+}$*) or *dnMAML$^{flox/+}$;Scgb1a1-CreER$^{TM/+}$;R26R$^{tdTomato/+}$* mouse lungs.

1410 5,000 cells of lineage-labelled secretory cells (EpCAM$^+$Tomato$^+$MHCII$^-$) isolated from

1411 *Scgb1a1-CreER$^{TM/+}$;R26R$^{tdTomato/+}$* or *dnMAML$^{flox/+}$;Scgb1a1-CreER$^{TM/+}$;R26R$^{tdTomato/+}$* mice

1412 were co-cultured with stromal cells with 1:5 ratio for 14 days. Each individual dot represents

1413 one individual experiment and data are presented as mean and s.e.m. Scale bar, 2,000μm. **j,**

1414 Representative IF images showing *Scgb1a1$^+$* lineage-labelled cells in a whole lobe of *Scgb1a1-*

1415 *CreER$^{TM/+}$;Red2-Notch$^{N1ICD/+}$* mice post tamoxifen treatment: YFP (yellow), RFP (red), pro-

1416 SPC (white, left), Scgb1a1 (white, right) and DAPI (blue). Scale bar, 500μm (left), and 100μm

1417 (right). Of note, only airway secretory cells were labelled by tamoxifen induction.

1418

1419
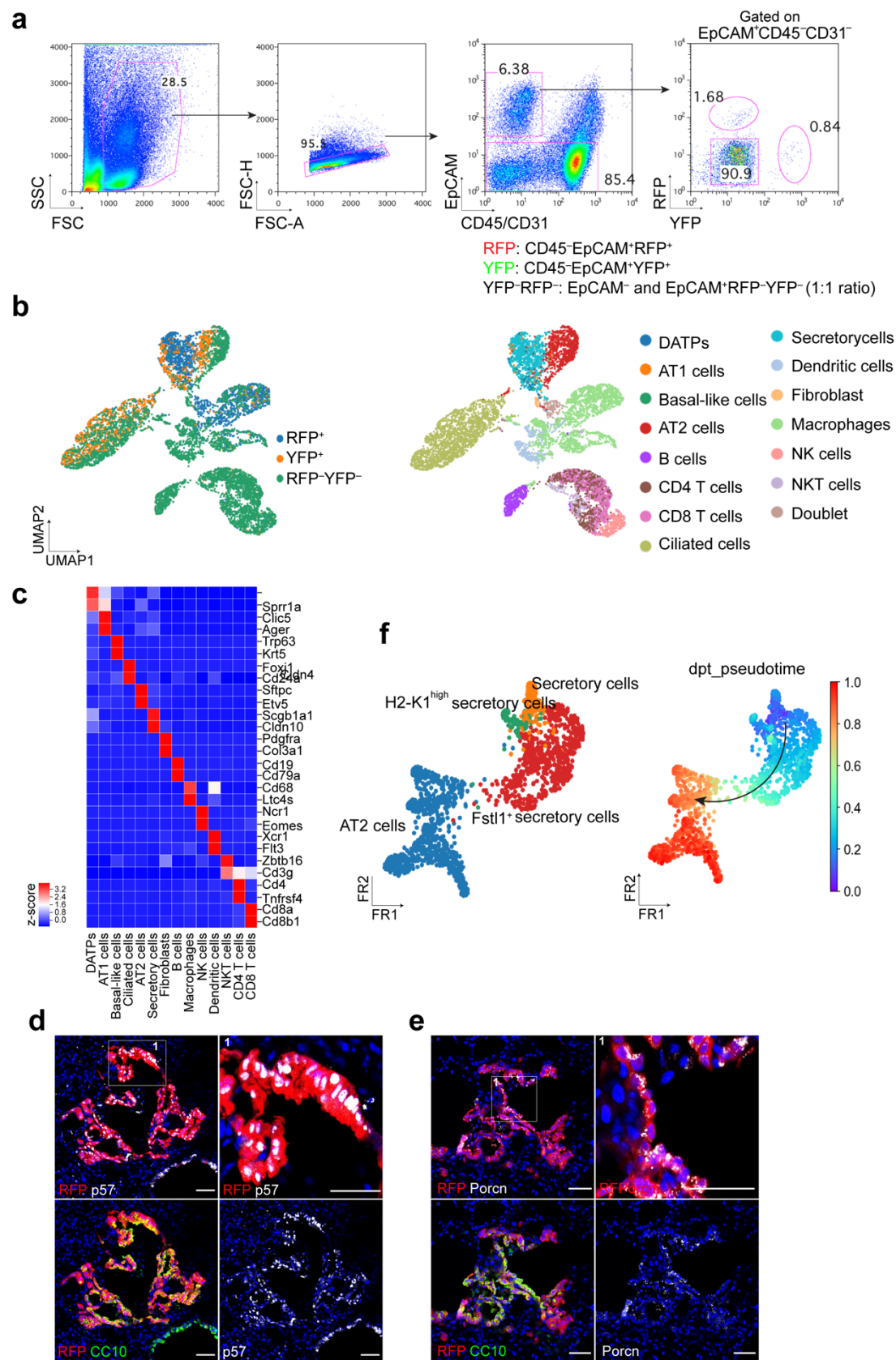
Extended Data Figure 6. scRNA-seq analysis of lung cells from *Scgb1a1-CreER^{TM/+}*;*Red2-Notch^{N1ICD/+}* mice at day 28 post bleomycin injury

1422   **a,** Sorting strategy for *Scgb1a1* lineage-labelled RFP$^+$ and YFP$^+$ or unlabelled (YFP$^-$RFP$^-$)

1423   cells by flow cytometry after bleomycin injury. For unlabelled population (YFP$^-$RFP$^-$),

1424   EpCAM$^-$RFP$^-$YFP$^-$ (non-epithelial population) and EpCAM$^+$RFP$^-$YFP$^-$ (epithelial

1425   population) cells were mixed at 1:1 ratio. **b,** Clusters of cell population after bleomycin injury

1426   from 10x Genomics 3' scRNA-seq analysis visualised by UMAP, assigned by specific colours.

1427   **c,** A heatmap showing gene expression patterns of key markers in each distinctive cell cluster.

1428   **d, e,** Representative IF images showing the expansion of Porcn$^+$ or p57$^+$ cells derivation from

1429   RFP$^+$ cells at day 28 post bleomycin injury. RFP (red), CC10 (green), p57 (white, e), Porcn

1430   (white, f), and DAPI (blue). Insets (1) show high-power view. Scale bar, 50μm. **f,** Diffusion

1431   map according to diffusion pseudotime (DPT, right) order coloured by samples (left).

1432

60

1433
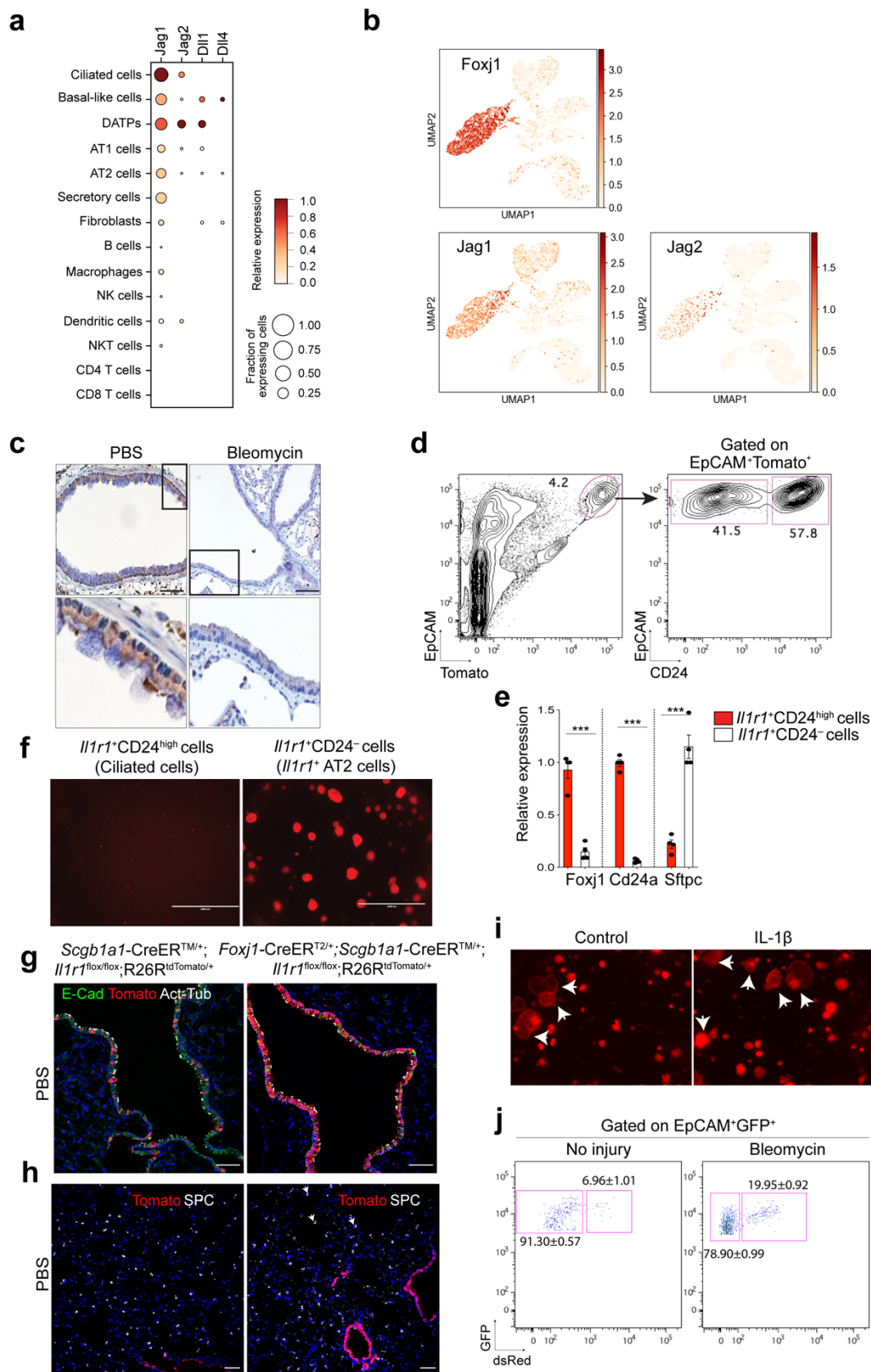
Extended Data Figure 7. Expression of Notch ligands in ciliated cells post alveolar injury

61

1435 **a,** Expression of Notch ligand in each distinctive cluster revealed in **Extended Data Fig. 6.**
1436 The size of the circle represents the fraction of cells expressing the gene and the colour
1437 represents the relative expression of each gene. **b,** UMAP visualisation of the log-transformed
1438 ($\log_{10}$(TPM+1)), normalised expression of selected marker genes (*Jag1* and *Jag2* for Notch
1439 ligand expression; *Foxj1* for ciliated cells) in distinctive clusters. **c,** Representative IHC images
1440 stained with anti-Jag1 in the distal airway of lungs from *Scgb1a1-CreER^{TM/+};R26R^{tdTomato/+}*
1441 mice at day 14 post PBS or bleomycin treatment. Insets (top) show high-power view (bottom).
1442 Scale bars, 50μm. **d,** Sorting strategy for *Il1r1^+* lineage-labelled ciliated
1443 (EpCAM^+Tomato^+CD24^high) and AT2 (EpCAM^+Tomato^+CD24^−) cells from *Il1r1-CreER^{T2/+};*
1444 *R26R^{tdTomato/+}* mouse lungs at day 4 post tamoxifen injection. **e,** qPCR analysis of *Foxj1, Cd24,*
1445 *and Sftpc* expression in isolated cells in (**d**). Each individual dot represents one individual
1446 experiment and data are presented as mean ± s.e.m. ***p<0.001. **f,** Representative fluorescent
1447 images of organoids derived from *Il1r1* lineage-labelled ciliated (*Il1r1^+*CD24^high) or AT2
1448 (*Il1r1^+*CD24^−) cells. Ciliated cells are unable to form organoids. Scale bars, 2,000μm. **g,**
1449 Representative IF images showing intact ciliated cells in the lungs of *Il1r1^{flox/flox};Foxj1-*
1450 *CreER^{T2/+};Scgb1a1-CreER^{TM/+};R26R^{tdTomato/+}* mice compared to those in the lungs of control
1451 *Il1r1^{flox/flox};Scgb1a1-CreER^{TM/+};R26^{RtdTomato/+}* mice: Tomato (for *Scgb1a1* or *Foxj1* lineage,
1452 red), Acetylated Tubulin (Act-Tub, white), E-Cadherin (E-Cad, green), and DAPI (blue). Scale
1453 bars, 50μm. **h**, Representative IF images showing a small number of *Scgb1a1* lineage-labelled
1454 AT2 cells at day 28 post PBS treatment in *Scgb1a1-CreER^{TM/+};Il1r1^{flox/flox};R26R^{tdTomato/+}* or
1455 *Foxj1-CreER^{T2/+};Scgb1a1-CreER^{TM/+};Il1r1^{flox/flox};R26R^{tdTomato/+}* mice. Tomato (for *Scgb1a1*
1456 lineage, red), SPC (white), and DAPI (blue). Arrowheads point to lineage-labelled SPC^+ AT2
1457 cells. Scale bar, 100μm. **i,** Representative fluorescent images of organoids derived from
1458 lineage-labelled secretory cells of *Scgb1a1-CreER^{TM/+};R26R^{tdTomato/+}* lungs. Organoids were
1459 cultured with PBS or IL-1β for 14 days. Arrows point to cystic airway-like organoids. Scale
1460 bar, 2,000μm. **j,** Flow cytometry analysis of secretory cell-derived AT2 cells isolated from
1461 *Scgb1a1-CreER^{TM/+};R26R^{fGFP/+};Sftpc-dsRed^{IRES-DTR/+}* mouse lungs after PBS (left) or
1462 bleomycin (right) treatment. Data are presented as mean ± s.e.m (n=2 individual biological
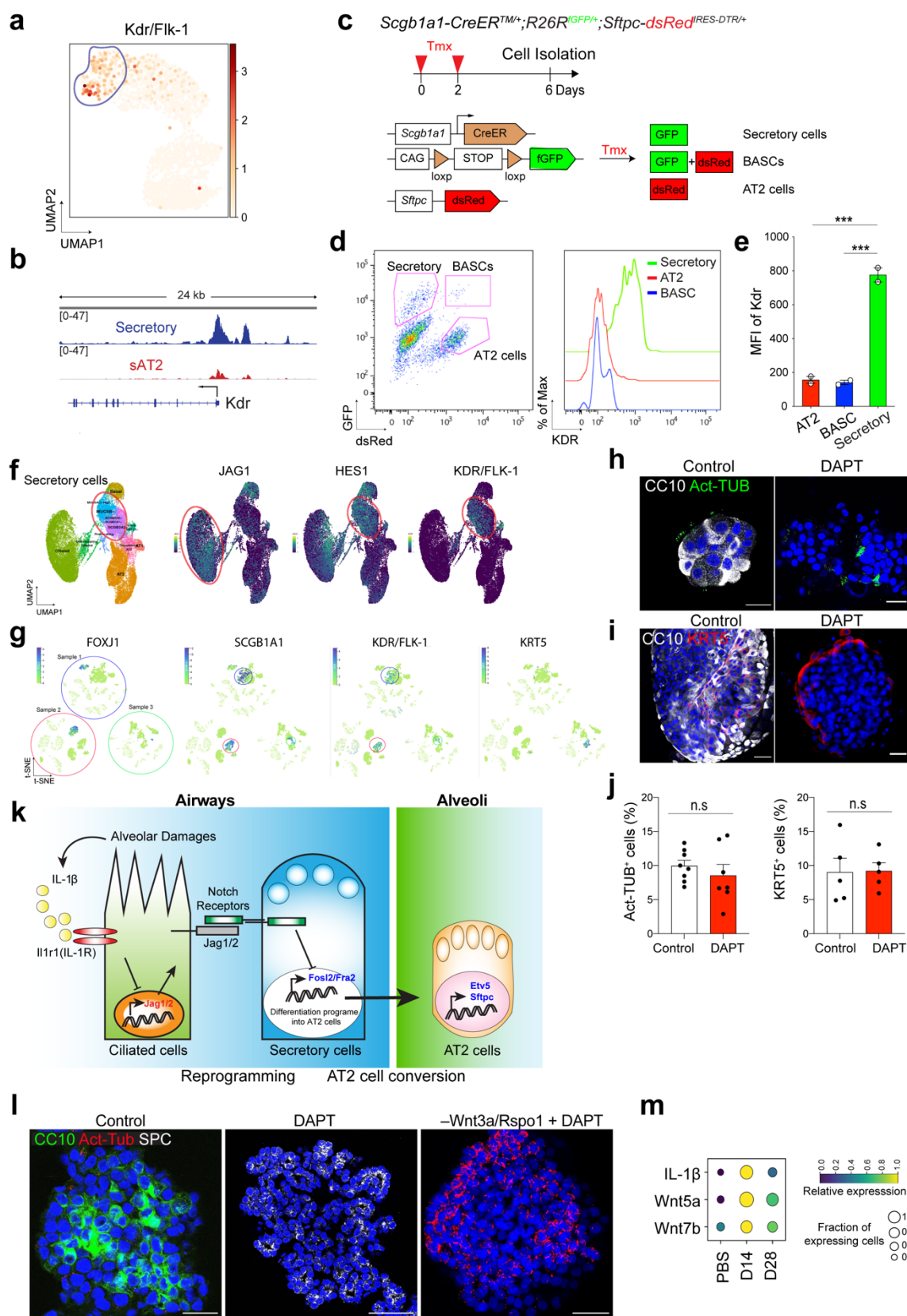1463 replicate).

1464

62
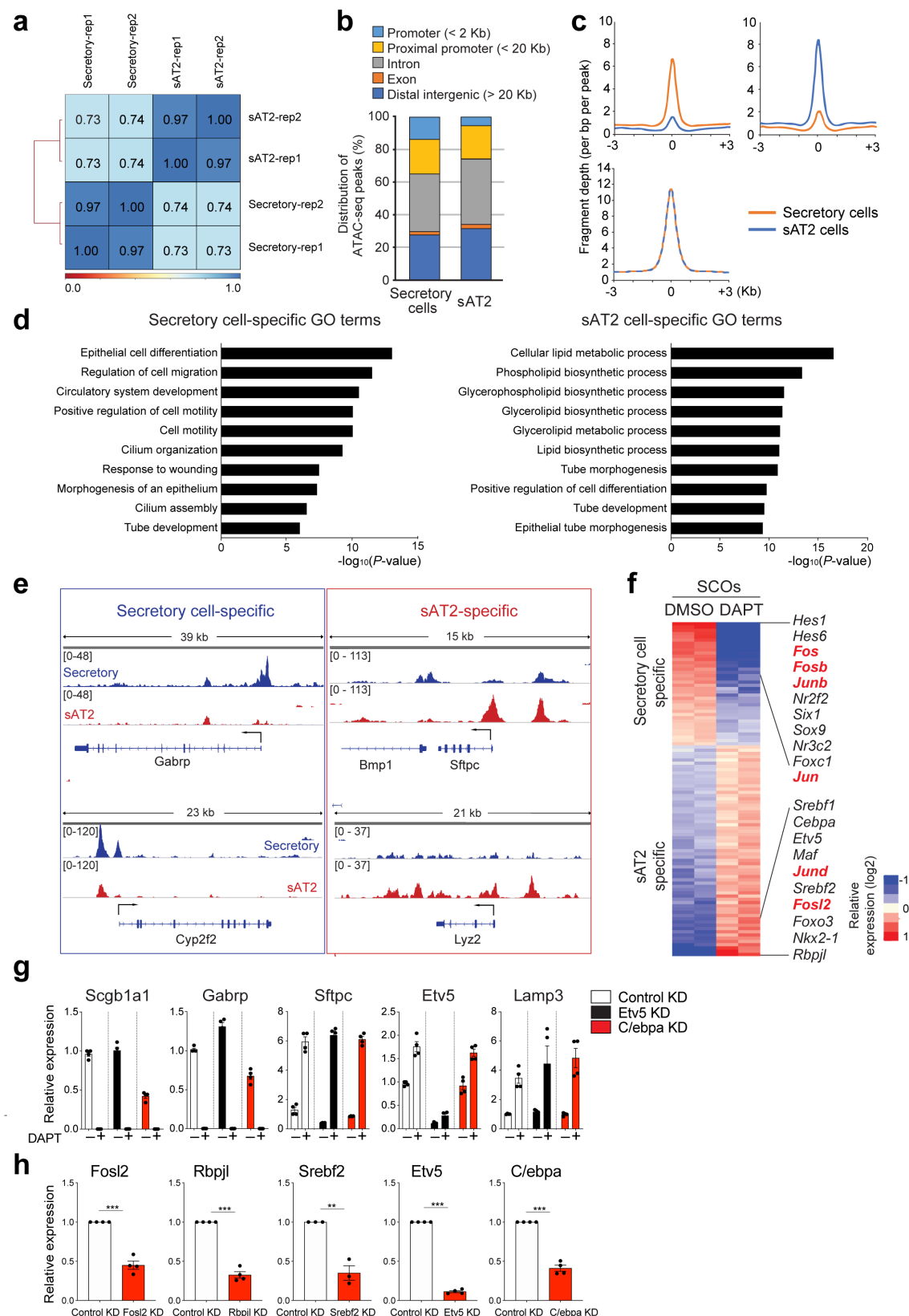
1465

Extended Data Figure 8. Differential genetic and epigenetic characteristics between secretory cells and secretory-derived AT2 (sAT2) cells.

1466

1467

1468   **a,** A spearman correlation map plotted by using ATAC-seq replicates obtained from secretory

1469   and sAT2 cells. **b**, A bar graph showing the chromosomal distribution of secretory-specific and

1470   sAT2-specific cis-regulatory elements, mapped by ATAC-seq in secretory and sAT2 cells

1471   across the mouse genome. **c,** The distribution of ATAC-seq peak signals in secretory and sAT2

1472   cells near the centre of secretory-specific, shared, and sAT2-specific open regions. **d**, Bar

1473   graphs showing enriched GO terms of the genes nearby secretory and sAT2-specific ATAC-

1474   seq peaks, respectively. **e,** Signal track images showing open chromatin regions nearby markers

1475   for secretory (*Gabrp* and *Cyp2f2*) and AT2 cells (*Sftpc* and *Lyz2*) in secretory (blue) and sAT2

1476   cells (red). **f,** A heatmap showing differentially expressed transcription factors (TFs) in

1477   secretory-derived organoids with or without DAPT treatment. **g,** qPCR analysis of the markers

1478   for secretory (*Scgb1a1* and *Gabrp*) and AT2 cells (*Sftpc*, *Etv5*, and *Lamp3*) in secretory cell-

1479   derived organoids (SCOs) with or without DAPT treatment after knockdown of control (white),

1480   *Etv5* (black), or *Cebpa* (red). **h,** qPCR analysis to confirm the knockdown efficiency of the

1481   genes that are used for indicated constructs in SCOs. Each individual dot represents one

1482   individual biological experiment (n=4 for knockdown of Fosl2, Rpbjl, Etv5, and C/ebpa, n=3

1483   for knockdown of Srebf2) and data are presented as mean ± s.e.m. **p<0.01, ***p<0.001.

1484

1485
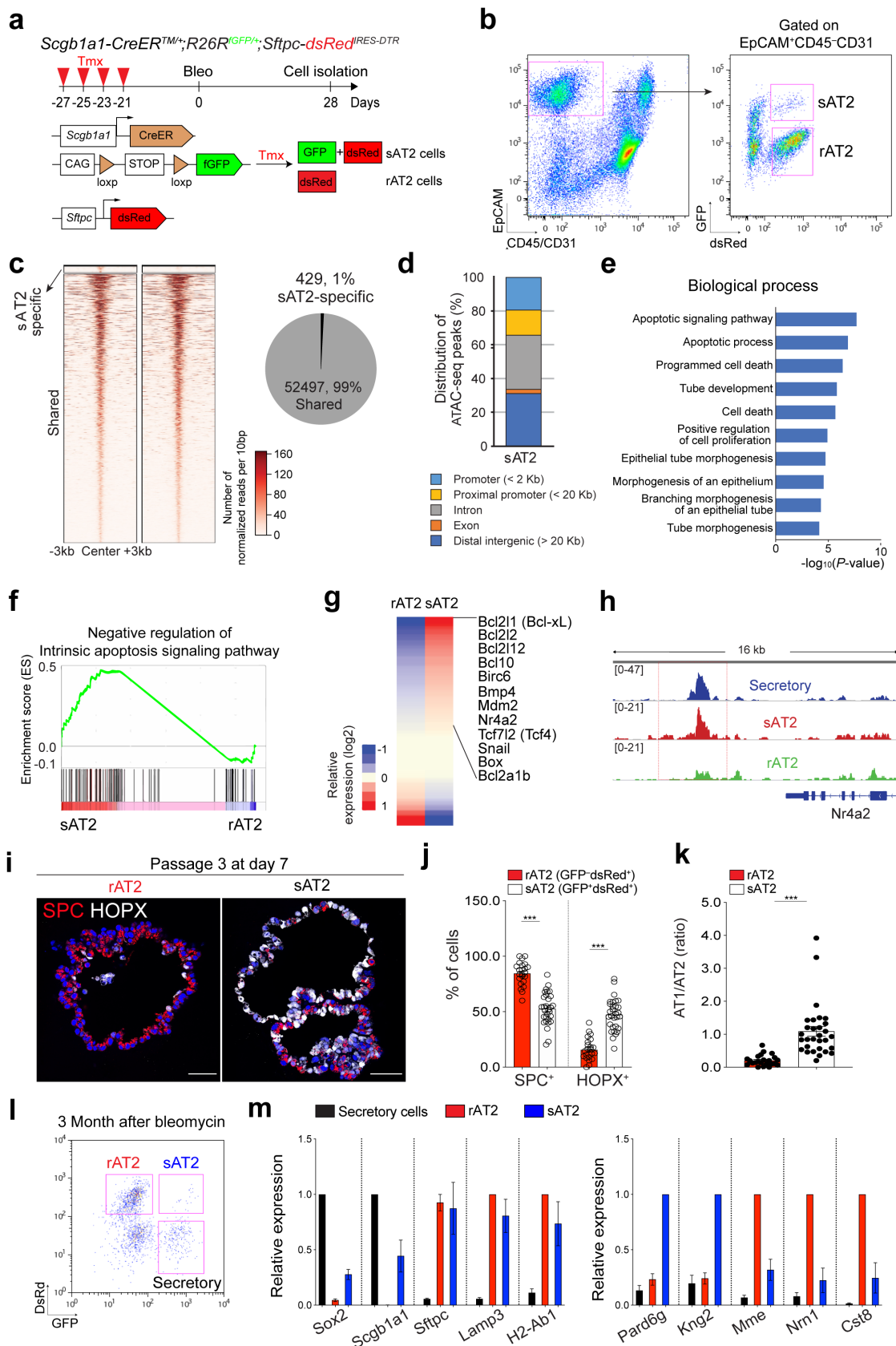
1486 **Extended Data Figure 9**. **Genetic and epigenetic differences of sAT2 cells compared to**

1487 **rAT2 cells**.

1488   **a,** Experimental design for isolation of secretory-derived (sAT2, GFP$^+$dsRed$^+$) and resident

1489   AT2 cells (non-lineage-labelled AT2, rAT2, GFP$^-$dsRed$^+$) using *Scgb1a1-CreER$^{TM/+}$*;

1490   *R26R$^{fGFP/+}$*;*Sftpc-dsRed$^{IRES-DTR/+}$* mice. Specific time points for tamoxifen injection and

1491   isolation are indicated. **b,** Representative flow cytometry analysis for isolation of sAT2

1492   (GFP$^+$dsRed$^+$) and rAT2 (GFP$^-$dsRed$^+$) cells. **c,** Heatmaps showing open chromatin regions

1493   specific in sAT2 cells and shared open chromatin regions between sAT2 cells and rAT2 cells

1494   (left). A pie chart presenting the proportion of sAT2-specific (blue) and shared regions (grey)

1495   (right). **d,** A bar graph showing the chromosomal distribution of sAT2-specific ATAC-seq

1496   peaks mapped in (**c**). **e,** A bar graph showing enriched GO terms of the genes nearby sAT2-

1497   specific peaks. **f,** GSEA with gene sets representing the negative regulation of intrinsic

1498   apoptosis signalling pathway in scRNA-seq data of sAT2 and rAT2 shown in Fig. 6a. **g,** A

1499   heatmap showing the expression patterns of the genes belonging to the negative regulation of

1500   apoptosis signalling pathway in sAT2 and rAT2 cells monitored by scRNA-seq (Fig. 6a). **h,**

1501   Signal track image showing open regions for *Nr4a2*, anti-apoptotic pathway marker, in

1502   secretory (blue), sAT2 (red), and rAT2 cells (green). **i,** Representative IF images of organoids

1503   derived from rAT2 or sAT2 cells. SPC (for AT2 cells, red), HOPX (for AT1 cells, white), and

1504   DAPI (blue). Scale bars, 50μm. **j, k,** Quantification of the frequency of AT2 (SPC$^+$) or AT1

1505   (HOPX$^+$) cells (**b**) and the ratio of AT1/AT2 cells (**c**) in rAT2- or sAT2-derived organoids.

1506   Each individual dot represents one organoid and data are presented as mean ± s.e.m (n=2

1507   independent biological replicates). ***p<0.001. **l,** Flow cytometry analysis of *Scgb1a1$^+$*

1508   lineage-labelled AT2 cells isolated from *Scgb1a1-CreER$^{T2/+}$*;*R26R$^{fGFP/+}$*;*Sftpc-dsRed$^{IRES-DTR/+}$*

1509   mouse lungs at 3 months after bleomycin injury. **m,** qPCR analysis of the genes in isolated

1510   secretory, rAT2, or sAT2 cells. Data are presented as mean ± s.e.m (n=4 individual mice).

1511

1512

Extended Data Figure 10. Identification of KDR/Flk-1 as a new surface marker of secretory cells in both mouse and human lungs.

67

1515   **a,** UMAP visualisation of the log-transformed ($\log_{10}$(TPM+1)), normalised expression of

1516   Kdr/Flk-1 in distinctive clusters shown in **Fig. 3j**. **b,** A signal track image showing open regions

1517   nearby *Kdr* mapped in secretory (blue) and sAT2 cells (red). **c,** Experimental design for

1518   isolation of CC10$^+$SPC$^-$ secretory cells, CC10$^+$SPC$^+$ dual-positive cells including

1519   Bronchioalveolar stem cells (BASCs), and CC10$^-$SPC$^+$ AT2 cells from *Scgb1a1-*

1520   *CreER$^{TM/+}$;R26R$^{fGFP/+}$;Sftpc-dsRed$^{IRES-DTR/+}$* mice. Specific time points for tamoxifen injection

1521   and isolation are indicated. **d,** Representative flow cytometry analysis (left) for isolation of

1522   secretory (GFP$^+$dsRed$^-$), BASCs (GFP$^+$dsRed$^+$), and AT2 (GFP$^-$dsRed$^+$) cells. KDR

1523   expression was determined by flow cytometry (right). **e,** A bar graph showing MFI (mean

1524   fluorescence of intensity) of KDR expression in indicated populations. Each individual dot

1525   represents one individual experiment and data are presented as mean ± s.e.m. ***$p<0.001$. **f,g,**

1526   UMAP (**f**) or t-SNE (**g**) visualisation of the normalised expression of *JAG1, HES1*, and *KDR*

1527   in distinctive human lung cell clusters from the dataset of Habermann et al.,[44](**f**) or Travaglini

1528   et al.,[45](**g**). *JAG1* is highly expressed in ciliated cells. Secretory cells express higher expression

1529   levels of *HES1* and *KDR*. **h,i,** Representative IF images of secretory cell-derived organoids

1530   retaining Act-Tub+ ciliated cells (**h**) and KRT5+ basal cells (**i**) treated with DMSO or DAPT

1531   (20μM). CC10 (white), Acetylated Tubulin (Act-Tub, green, **h**), KRT5 (red, **i**), and DAPI

1532   (blue). Scale bar, 50μm. **j,** Quantification of the frequency of Act-Tub$^+$ ciliated cells or KRT5$^+$

1533   basal cells in control or DAPT-treated organoids. Each individual dot represents one organoid

1534   and data are presented as mean ± s.e.m (n=3 independent experiments). n.s.=not significance.

1535   **k**, Notch inhibition coordinates the cell fate decision of secretory cells into AT2 cells in two

1536   stages: 1) Reprogramming; loss of secretory cell identity and 2) AT2 cell conversion;

1537   acquisition of transcriptional programmes for AT2 cell differentiation vis the transcription

1538   regulator *Fosl2*. Pro-inflammatory cytokine IL-1β driven by tissue injury regulates the

1539   expression of Notch ligands such as Jag1/2 in ciliated cells, which induces the downregulation

1540   of Notch activity in secretory cells localised adjacent to ciliated cells. Fosl2/Fra2-mediated AP-

1541   1 factor triggers the differentiation programmes of secretory cells to enter AT2 cell

1542   differentiation process during alveolar regeneration. **l,** Representative IF images of secretory

1543   organoids treated with DMSO (control) or DAPT (20μM) in the presence (middle) or

1544   withdrawals of Wnt-inducing factors (right). Organoids were cultured in the medium

1545   supplemented with Wnt3a/Rspo1 for 7 days and then DAPT was treated for further 7 days with

1546   or without Wnt3a/Rspo1. CC10 (for secretory cells, green), Acetylated Tubulin (for ciliated

1547   cells, Act-Tub, red), SPC (for AT2 cells, white), and DAPI (blue). Scale bars, 50μm. **m,** The

1548   expression of *IL-1β, Wnt5a,* and *Wnt7b* at indicated time points after bleomycin injury. Data

1549   were from our previous study[30].